ICARUS 76, 404–436 (1988)

The 2.5–12 μm Spectrum of Comet Halley from the IKS–VEGA Experiment

M. COMBES,* V. I. MOROZ,† J. CROVISIER,* T. ENCRENAZ,* J.-P. BIBRING,‡ A. V. GRIGORIEV,† N. F. SANKO,† N. CORON,§ J. F. CRIFO,§ R. GISPERT,§ D. BOCKELÉE-MORVAN,* YU. V. NIKOLSKY,† V. A. KRASNOPOLSKY,† T. OWEN,# C. EMERICH,§ J. M. LAMARRE,§ AND F. ROCARD‡

Observatoire de Paris, F-92195 Meudon, France; †Space Research Institute, Profsoyuznaya, 84/32, 117810 Moscow GSP-7, USSR; ‡Laboratoire René Bernas, BP No. 1, F-91406 Orsay, France; §Laboratoire de Physique Stellaire et Planétaire, BP No. 10, F-91370 Verrières-le-Buisson, France; and #ESS Department, State University of New York, Stony Brook, New York 11794

Received November 25, 1987; revised March 22, 1988

The infrared instrument IKS flown on board the VEGA space probes was designed for the detection of emission bands of parent molecules, and for a measurement of the size and temperature of the thermal emitting nuclear region. The instrument had three channels with cooled detectors: an "imaging channel" designed to modulate the signal of the nucleus and two spectroscopic channels operating at 2.5–5 and 6–12 μm, respectively, equipped with circular variable filters of resolving power ~50. This paper presents and discusses the results from the spectral channels. On VEGA 1, usable spectra were obtained at distances D from the comet nucleus ranging from 250,000 to 40,000 km corresponding to fields of view 4000 and 700 km in diameter, respectively. The important internal background signal caused by the instrument itself, which could not be cooled, had to be eliminated. Since no sky chopping was performed, we obtain difference spectra between the current spectrum and a reference spectrum with little or no cometary signal taken at the beginning of the observing sequence (D ~ 200,000 km). Final discrimination between cometary signal and instrumental background is achieved using their different time evolution, since the instrumental background is proportional to the slow temperature drift of the instrument, and the cometary signal due to parent molecules or dust grains is expected to vary in first order as D^{-1}.

The 2.5–5 μm IKS spectra definitely show strong narrow signals at 2.7 and 4.25 μm, attributed to the ν_3 vibrational bands of H_2O and CO_2, respectively, and a broader signal in the region 3.2–3.5 μm, which may be attributed to CH-bearing molecules. All these signals present the expected D^{-1} intensity variation. Weaker emission features at 3.6 and 4.7 μm could correspond to the ν_1 and ν_5 bands of H_2CO and the (1 − 0) band of CO, respectively. Molecular production rates are derived from the observed emissions, assuming that they are due to resonance fluorescence excited by the Sun's infrared radiation. For the strong bands of H_2O and CO_2, the rovibrational lines are optically thick, and radiative transfer is taken into account. We derive production rates, at the moment of the VEGA 1 flyby, of ~10^{30} sec^{-1} for H_2O, ~2.7×10^{28} sec^{-1} for CO_2, ~5×10^{28} sec^{-1} for CO, and 4×10^{28} sec^{-1} for H_2CO, if attributions to CO and H_2CO are correct. The production rate of carbon atoms in CH-bearing molecules is ~9×10^{29} sec^{-1} assuming fluorescence of molecules in the gas phase, but could be much less if the 3.2–3.5 μm emission is attributed to C–H stretch in polycyclic aromatic hydrocarbons or small organic grains. In addition, marginal features are present at 4.85 and 4.45 μm, tentatively attributed to OCS and molecules with the CN group, respectively. Broad absorption at 2.8–3.0 μm, as well as a narrow emission at 3.15 μm, which follow well the D^{-1} intensity variation, might be due to water ice. Emission at 2.8 μm is also possibly present, and

0019-1035/88 $3.00

might be due to OH created in vibrationally excited states after water photodissociation. The 6–12 μm spectrum does not show any molecular emission, nor emission in the 7.5-μm region. The spectrum is dominated by silicate emission showing a double structure with maxima at 9.0 and 11.2 μm, which suggests the presence of olivine.

1. INTRODUCTION

One of the main goals of cometary studies is the determination of the composition of the volatile species contained in the nucleus. These species were condensed during or before the formation phase of comets. If one excepts the nucleus surface exposed to cosmic rays and stellar ultraviolet, these species are believed to remain mostly unchanged since that time due to the cold temperature of these bodies and to their small sizes, which preclude any metamorphic process. Therefore, the interior of cometary nuclei may be considered as pristine materials representative of the primitive solar nebula, and witnesses of the formation of Solar System bodies from interstellar matter.

When a comet enters the inner Solar System, the volatile species are released by solar heating and form an atmosphere that can be studied by the usual remote-sensing techniques. Unfortunately, visible spectroscopy, which has been applied to comets for more than a century, is of little help to determine the nature of nucleus volatile species ("parent molecules") because these species generally do not have spectral signatures in the visible, and they are readily destroyed by photolytic processes due to the solar UV radiation. This technique revealed only secondary products, namely, radicals ("daughter molecules"), atoms, and ions. Among the species observed by the recent UV spectroscopy of comets, only the CO and S_2 molecules may directly originate from the nucleus.

Since most parent species do not have strong electronic transitions in the visible or UV spectral ranges, one has to search for these species in the near- and medium-infrared (vibrational transitions) or microwave and far-infrared (pure rotation transitions) ranges. Such searches are difficult since (i) the corresponding techniques are recent and still difficult to handle; (ii) the transition energies are low; and (iii) the Earth's atmosphere is opaque in a large part of these spectral ranges, which implies high-altitude or even orbital observations. This explains why, before the comet Halley observing campaign in 1985–1986, infrared and radio observations of comets had not revealed any signal from parent molecules, if one excepts a few unconfirmed tentative detections.

Prospective theoretical works were undertaken these last years to study the possible excitation mechanisms of parent cometary molecules in the gaseous phase. They came to the conclusion that the main emission mechanism should be resonant fluorescence of the fundamental vibrational bands, induced by the solar infrared radiation field (Encrenaz *et al.* 1982, Yamamoto 1982, Crovisier and Encrenaz 1983, Weaver and Mumma 1984). Synthetic infrared spectra of the overall emission of these bands at medium spectral resolution were published, but more detailed studies of individual molecules are also available (CO: Crovisier and Le Bourlot 1983, Chin and Weaver 1984; HCN and CN-bearing molecules: Bockelée-Morvan *et al.* 1984, Bockelée-Morvan and Crovisier 1985; linear molecules in general: Crovisier 1987; H_2O: Bockelée-Morvan and Crovisier 1986, Bockelée-Morvan 1987, Bisikalo *et al.* 1987).

We present here the results of a search for parent molecules at infrared wavelengths (2.5–12 μm) in comet Halley during its encounter by the two VEGA spacecraft.

These flybys offered a unique opportunity for such an investigation, compared with Earth-based observations, because (i) there is no limitation due to atmospheric transmission; (ii) the signal is much stronger due to the proximity of the comet; and (iii) one can sample the inner coma where the parent molecules are not yet photodestroyed. On the other hand, the sensitivity of such a spaceprobe-borne IR experiment was limited by the impossibility of cooling detectors at liquid helium temperature and using efficient sky chopping once the craft were inside the coma. The instrument, named IKS (from the initials of the Russian translation for "infrared spectrometer"), was a small telescope equipped with two medium-resolution spectrometric channels operating in the ranges 2.5–5 and 6–12 μm. These ranges cover most of the strongest vibrational bands of suspected parent molecules such as H_2O, CO, CO_2, CH_4, H_2CO, NH_3. They are also adequate for the study of broad features from dust and ice particles. The instrument was additionally equipped with an "imaging channel," designed to measure the size and temperature of the nucleus. The results of this part of the experiment are described elsewhere (Emerich *et al.* 1987, Nikolsky *et al.* 1987).

The IKS experiment worked successfully during the VEGA 1 flyby of comet Halley. The presence of the signature of H_2O, CO_2 and CH-bearing molecules in the 2.5–5 μm spectrum was obvious even in the quick-look analysis performed just after the flyby. Preliminary accounts of the results at various steps of their analysis were already published (Combes *et al.* 1986a,b,c,d, Moroz *et al.* 1987a,b). The goal of the present paper is to give a more complete and final presentation of the IKS instrument, its performance and operation, the data reduction, the results, and their analysis.

Section 2 describes the IKS instrument, its performance and its operation during the flybys. Sections 3 and 4 present the data processing procedures and the results of the short-wavelength channel (2.5–5 μm), and the long-wavelength channel (6–12 μm), respectively. In conclusion, Section 5 summarizes our main results and outlines the prospects of future infrared cometary observations.

2. THE INSTRUMENT, ITS PERFORMANCE AND ITS OPERATIONS

2.1 Instrument Description

The characteristics of the IKS instrument are summarized in Table I and in Fig. 1. They are presented in detail in Crifo (1981) and Arduini *et al.* (1982). The instrument is mounted on the pointing platform of the VEGA probe, continuously oriented toward the comet nucleus during the flyby phase. It consists of an f/3.8 baffled Ritchey–Chretien telescope with a primary mirror 140 mm in diameter. The field-of-view (FOV) diameter is 60 arcmin. The telescope itself, the transfer optics, and the filter wheel are not cooled. When in operation, the temperature is passively stabilized around 15°C. The collected light is divided into three secondary beams (Fig. 1). Each

TABLE I

Characteristics of the IKS Instrument and Parameters of the Encounter of P/Halley with the VEGA 1 Spacecraft

	Short-wavelength spectroscopic channel	Long-wavelength spectroscopic channel
Wavelength range	2.4–4.9 μm	6.0–12.0 μm
Spectral resolution, $\Delta\lambda$(FWHM)/λ	1/41 at 2.6 μm 1/70 at 4.8 μm	1/41 at 6.3 μm 1/66 at 11.3 μm
Sensitivity (rms noise in 18 sec)	2×10^{-8} W cm^{-2} sr^{-1} μm^{-1} at 3 μm	2×10^{-7} W cm^{-2} sr^{-1} μm^{-1} at 6 μm

Telescope diameter	140 mm
Field-of-view diameter	1°
Time to closest approach, T_0	6.306 Mar 1986 (UT)
Distance of closest approach	8890 km
Encounter velocity	79.2 km sec^{-1}
Sun–comet distance	0.79 AU
Earth–comet distance	1.15 AU

Useful observing sequence	Beginning	End
Time	T_0 − 55 min	T_0 − 8 min
Distance to comet	276,000 km	36,000 km
Field-of-view diameter	4,000 km	640 km

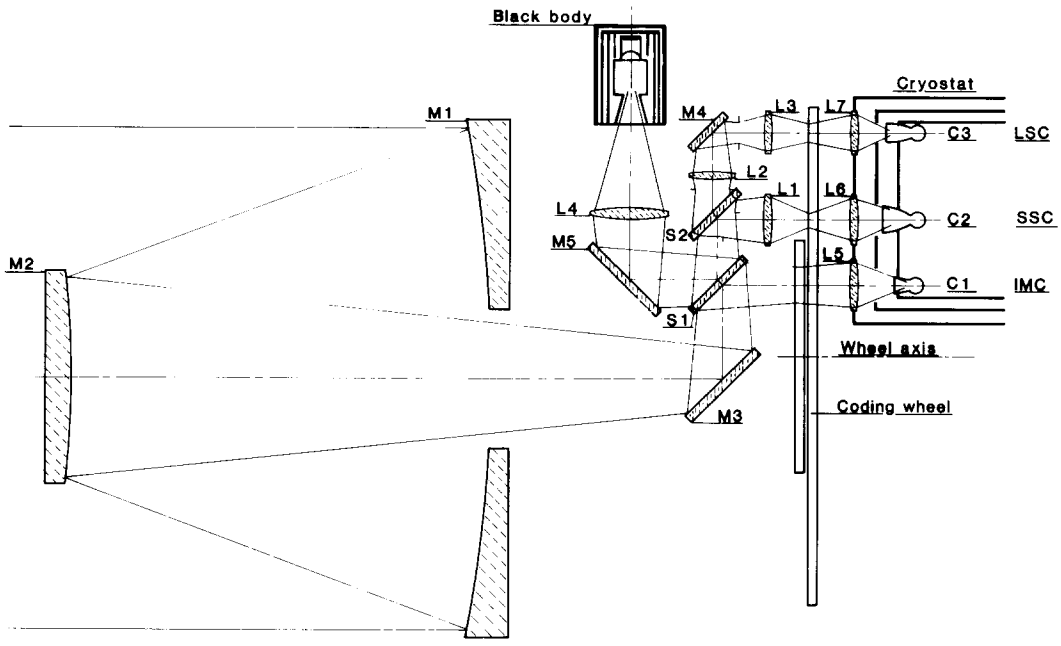

FIG. 1. Optical scheme of the IKS instrument. M1, M2: primary and secondary mirrors of the telescope. M3, M4, M5: folding mirrors. L1 to L7: germanium lenses. S1, S2: dichroic beam splitters. C1, C2, C3: detectors. LSC and SSC: long- and short-wavelength spectroscopic channels. IMC: imaging channel.

beam passes through one of the three tracks of a modulating filter wheel and is sent to a cryogenically cooled detector. One of the tracks, which is dedicated to the imaging channel, bears an encoding grid and broadband filters. The two other tracks are circular variable interference filters (CVFs). They operate in the range 2.5–5 μm (SSC, or short-wavelength spectrometric channel) and the range 6–12 μm (LSC, or long-wavelength spectrometric channel), respectively, with a practically constant resolution of $\Delta\lambda \sim 0.07$ μm for the SSC and $\Delta\lambda \sim 0.16$ μm for the LSC. This corresponds to a resolving power ranging from ~40 (at minimum λ) to ~70 (at maximum λ) on both channels.

The detectors are InSb and HgCdTe monodetectors for the SSC and LSC, respectively. Since their sensitivity is degraded by several orders of magnitude at room temperature, these detectors are enclosed in a cryostat and cooled to ~77 K during operation of the instrument. Cooling is achieved by Joule–Thompson expansion of nitrogen stored under 350 atm, allowing a cooling sequence of about 3 hr.

On each 360° track of the CVF, λ varies from λ_{min} to λ_{max}, and then to λ_{min} without any discontinuity. The signal is sampled at 180 points in each half-track, allowing no resolution degradation. To accommodate a large dynamic range, the continuum components of the spectra are electronically filtered out, and the continuum levels are recorded separately. The digitalized spectra are averaged over 128 wheel rotations, corresponding to 18 sec of observation, before being transmitted to Earth by telemetry.

Since no chopping other than spectral modulation is made, the recorded signal is expected to be dominated by instrumental background emission. Great care has been taken in the thermal design to ensure temperature stability. To monitor the temperature evolution of the instrument during the calibration tests and the observations, several thermometers are placed in various

spots of the instrument. In some critical points (such as the cryostat, or the CVF environment), high-accuracy thermometers are used. To have an absolute calibration at the moment of the flyby, a reference blackbody is incorporated into the instrument, the calibration sequence being programmed to take place at the end of the observation.

2.2. Preflight Calibration and Instrument Performance

Extensive preflight calibration of the IKS instrument was carried out (Bibring *et al.* 1984). The wavelength value versus the CVF angular position has been defined with an accuracy much better than the spectroscopic resolution. The transmission of the instrument versus wavelength has been measured as well as its absolute responsivity. The sensitivity of IKS (rms noise in an 18-sec integration spectrum) has been determined to be close to 2×10^{-8} W cm^{-2} sr^{-1} μm^{-1} at 3 μm and 2×10^{-7} W cm^{-2} sr^{-1} μm^{-1} at 6 μm, corresponding to a dynamic range of about 10^5. Nevertheless, as discussed in the following sections, the actual limitation on the signal-to-noise ratio is not due to the quite good sensitivity of the instrument, but to the limited accuracy of the cancellation of the instrumental background.

Indeed, the thermal emission of the instrument itself was expected to be largely dominant with respect to the cometary signal. The temperature of the cometary dust at the encounter was estimated to be close to 400 K. The dust particle size and number density distribution lead to a very low equivalent emissivity ($\sim 10^{-5}$). To improve the signal, the cometary flux is collected in a large field of view. In contrast, the instrumental signal is due mainly to the close-to-one reflectivity of the CVF and to the emissivity of its environment at a temperature of about 300 K. The effective bandpass for background collection, limited only by the 2.5–5 μm and 6–12 μm cold filters inside the cryostat, is much larger than the CVF bandpass ($\lambda/\Delta\lambda \sim 50$) which limits the recorded cometary signal. Moreover, due to optical scattering effects, the effective FOV for background collection is larger than the nominal 1° FOV. As a consequence, the background instrumental signal was expected to be 10^5 to 10^6 times larger than the cometary signal. Such a large factor is usual for infrared astronomical observations. The well-known and efficient beam modulation technique was not used on IKS. Indeed it was recognized that an on/off optical chopping inside the variable and unknown coma could not provide a 10^6 rejection factor; neither could an internal mechanical chopping which would have required an unachievable temperature stability at the encounter time, when the probe attitude with respect to the Sun has to change by 180° within some minutes.

Spectral modulation of the signal is achieved by fast rotation of the CVF. Since most of the background is coming from a zone located between the CVF itself and the cold filters inside the cryostat, the background component is mainly not modulated. Nevertheless, due to variations of the CVF reflectivity with angular position, a significant part of the instrumental signal is modulated as the cometary signal is and, as a consequence, detected by the electronics. As a result, the spectroscopic modulation could not reject more than 90% of the instrumental background.

The methods for removing the remaining background (see Sects. 3.1 and 4.1) were tested during the preflight calibration program. The main conclusion was that the remaining background depends primarily on the temperature of the CVF environment and partly on the temperature of the detector and cold-filter zone. These temperatures were continuously monitored during observations with high accuracy (some 10^{-2} K). Nevertheless, due to the high sensitivity of the instrument and/or to thermal inertia effects between the optical components and the thermometers, it was concluded that thermal modeling of the background using the temperature monitoring could not

be accurate enough for providing the best background cancellation. As explained in detail in Sections 3.1 and 4.1, the extraction of the cometary signal is possible, using the different time evolution of cometary signal and instrumental background.

2.3. Instrument Operation during Encounter

On VEGA 1, the instrument operated according to its specifications, except for two events. (i) 5 minutes before the encounter time T_0, it received an erroneous command that initiated the shutdown procedure, and data acquisition stopped at T_0 + 3 min. The instrument could be restarted at T_0 + 33 min by telecommand and worked until the end of the cooling sequence at T_0 + 50 min. (ii) Near the encounter (from T_0 − 8 min on), the temperature inside the cryostat was not stable for unknown reasons. Large variations in the background resulted, which did not affect the image channel results, but rendered unexploitable the spectroscopic channel data taken at that moment.

Therefore, usable data were recorded during two uninterrupted sequences (Fig. 2): (1) from T_0 − 55 min to T_0 − 8 min, when the probe approached the nucleus from 276,000 to 36,600 km (166 individual spectra) and (2) from T_0 + 33 min to T_0 + 50 min, when the probe returned from the nucleus from 162,000 to 222,000 km (52 individual spectra).

The parameters of the VEGA 1 flyby are summarized in Table I. The evolution of the temperatures recorded during the encounter at several points of the instrument is shown in Fig. 3.

On VEGA 2, no result could be obtained from IKS due to a failure of the cryogenic system.

3. The Spectrum from 2.5 to 5 μm

3.1. Data Processing

As stated above, since the telescope and CVF are not cooled, and since no chopping other than spectral modulation is used, the raw spectra are dominated by the very strong internal background signal. For the SSC, this latter is about 10^5 larger than the rms noise of the detectors in an 18-sec spectrum, and about 10^4 larger than the strongest expected molecular cometary signals. Our data retrieval procedure is based on the fact that the time variations of the internal background signal and of the cometary signal are different, the former being linked to the slow temperature drifts of the instrument, which were monitored, and the latter, to the spacecraft–comet distance.

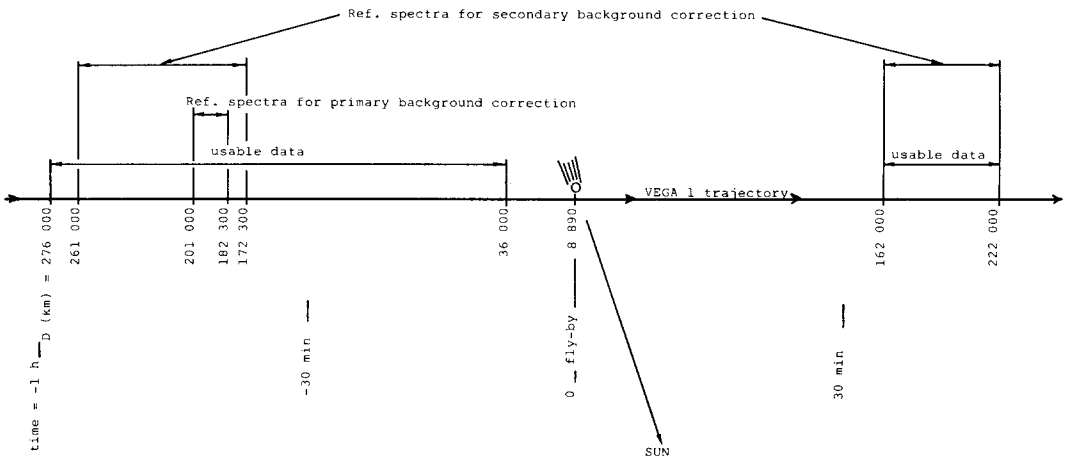

FIG. 2. Synopsis of VEGA 1 trajectory indicating where the different relevant spectra were taken.

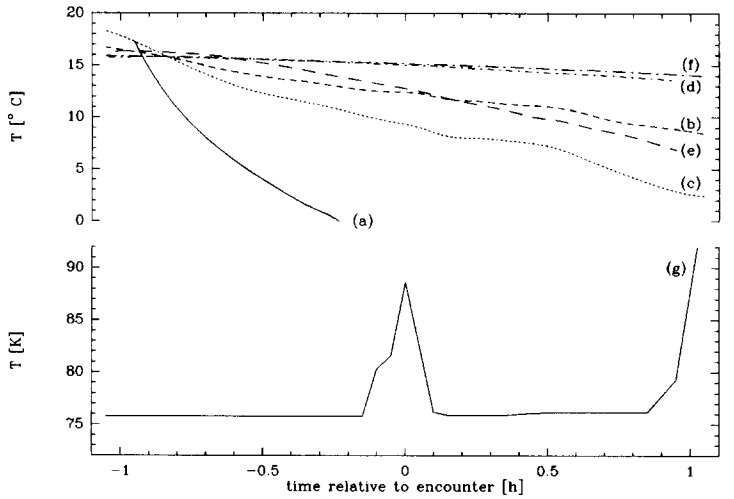

FIG. 3. Evolution of the temperatures taken at various places of the IKS instrument during the VEGA 1 encounter of comet Halley. (a) Telescope baffle, front region. (b) Telescope baffle, near primary mirror. (c) Spider. (d) Primary mirror. (e) Secondary mirror. (f) Filter wheel. (g) Detector.

The sequence of the different steps of the data reduction of the 2.5–5 μm channel is illustrated in Figs. 4a–e, which show how the last useful spectrum before closest encounter was processed. This spectrum, which contains the strongest cometary signal, corresponds to a distance D = 40,000 km to the comet nucleus.

A first-order correction is obtained by taking the difference between the current spectrum S_i and a reference spectrum S_R obtained at the beginning of the observing sequence, where the cometary signal is supposed to be small. Such reference spectra are typically taken at $D \sim 200{,}000$ km (Fig. 2). At that distance, the cometary signal is expected to be only one-fifth that at $D \sim 40{,}000$ km (Sect. 3.2.1): this will be taken into account in the subsequent analysis. In the resulting difference, 99% of the internal signal is removed (Fig. 4b).

The remaining background at this step, still dominating the spectrum, consists of two components: (a) a component that has the overall shape of the original internal signal (Fig. 4a) and that is smoothly varying with time—this is due to the slow temperature variations of the instrument, in particular, of the filter wheel (~2 K during the flyby observation sequence; Fig. 3) and (b) an additional modulation that is present in the region $\lambda < 3$ μm, with an intensity comparable to that of the expected signal of the water band. This modulation is correlated with very small variations of the internal temperature of the cryostat, which was monitored by a high-sensitivity thermometer with a precision of 10^{-2} K (Fig. 3). Nevertheless, such quite good accuracy is not sufficient to allow a direct correction.

As can be seen in Fig. 4b, the shape of component a shows two extrema at 3.50 and 4.82 μm. Thus, it may be parameterized for the $S_x(\lambda)$ spectrum by

$$u_a(x) = S_x(4.82\ \mu\text{m}) - S_x(3.50\ \mu\text{m})$$

which describes its amplitude. In the same way, component b can be parameterized by:

$$u_b(x) = S_x(2.35\ \mu\text{m}) - 0.5\,[S_x(2.45\ \mu\text{m}) + S_x(2.59\ \mu\text{m})].$$

An attempt to correct simultaneously for both components can be made in the following way. For the current spectrum difference $[S_i - S_R]$, we look for an associated

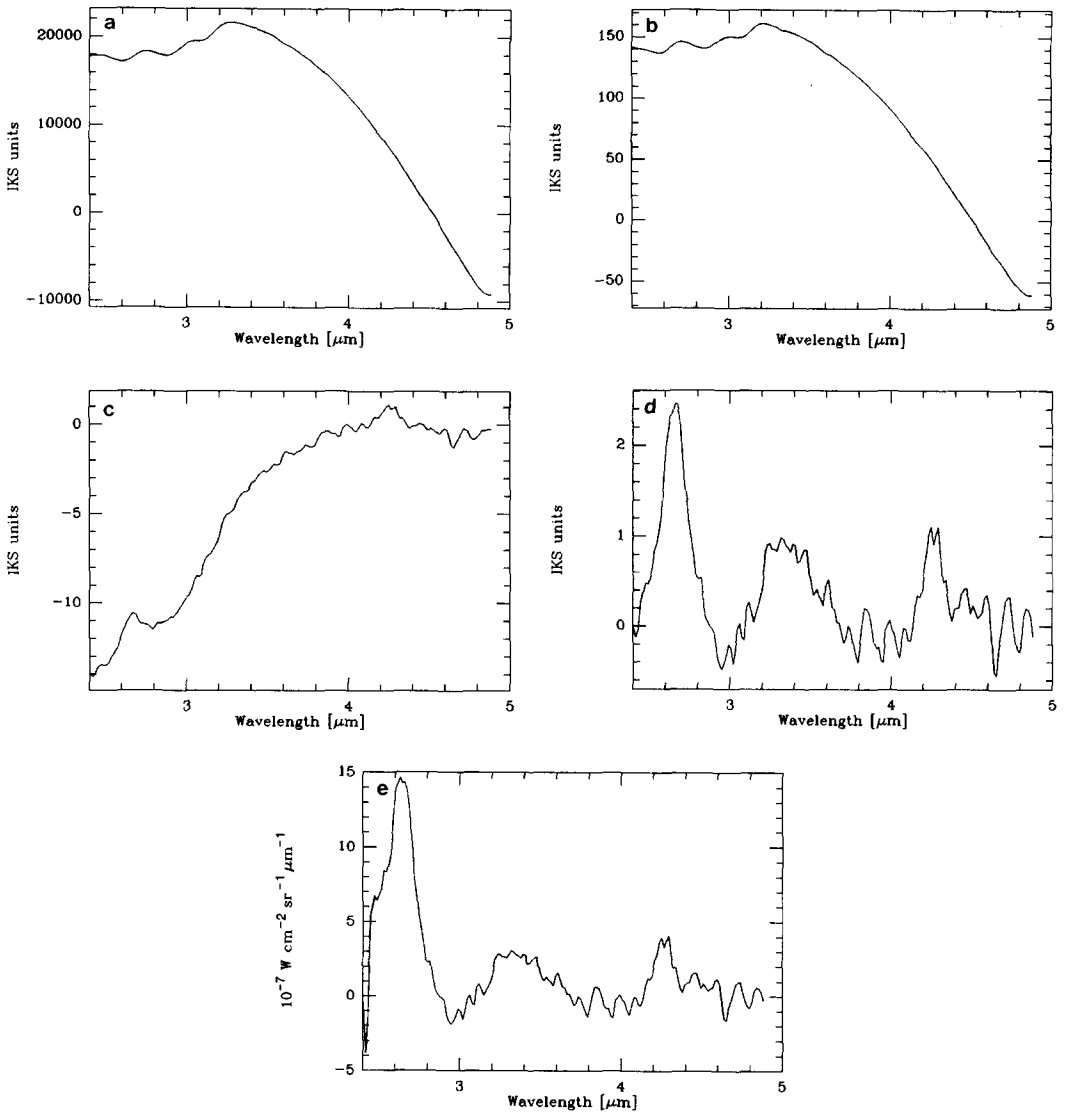

FIG. 4. The different steps of data processing, from the raw spectrum to the calibrated spectrum with internal background signal removed (see Section 3.1). The procedure is illustrated here on the last useful spectrum obtained before closest approach. (a) Raw spectrum. (b) First-order correction. (c) Second-order correction. (d) Removal of a fourth-order baseline. (e) Application of the transmission correction.

pair of spectra (S_j, S_k), S_j and S_k being taken in the useful sequences obtained respectively before and after closest encounter (Fig. 2), both at large and similar distances from the comet. We choose S_j and S_k such that the difference $S_j - S_k$ has a and b background components similar to those of the $S_i - S_R$ difference. In other words, we look for a difference $S_j - S_k$ for which u_a/u_b is as close as possible to that of $S_i - S_R$. It is then possible to obtain a spectrum corrected to the second order:

$$S_i^{corr} = [S_i - S_R] - c[S_j - S_k]$$

for which u_a and u_b are zero. Practically, the correction factor c is fairly small, on the order of 0.2. Because of this and of the fact that S_j and S_k are taken at approximately the same large distance from the comet, the spurious cometary signal that might be added in this second step of background correction is small (at most 5% of the cometary signal observed at 40,000 km).

It must be noted that this correction is not always possible, depending on both S_i and S_R. For a given S_i we tried several S_R in a limited range of distances (Fig. 2). When several S_R appear to be suitable, we average the resulting corrected spectra. Several S_i, for which it was not possible to find any correction at all, had to be eliminated. But 103 out of the 163 spectra of the sequence obtained before closest encounter have been treated in this way, most of the eliminated spectra being concentrated at the beginning of the sequence, at large distances from the comet and therefore containing less information.

After this second-order correction, the spectra clearly show some narrow features which could be attributed to cometary molecular emission (Fig. 4c). However, they still contain a continuum component that is not likely to be of cometary origin, but rather is caused by the imperfection of our background removal procedure. To extract the narrow molecular signals, several procedures have been employed: a Fourier-transform filtering of the low frequencies (Combes *et al.* 1986a), and the subtraction of a polynomial baseline (Combes *et al.* 1986c, Moroz *et al.* 1987a,b). Another method, based on adapted filtering of the expected molecular spectral features, will be presented in Section 3.2.1. All these methods lead to consistent results for narrow features. The spectra presented in Figs. 5 and 6 and analyzed in Section 3.2 (see also Figs. 4d and e) result from the subtraction of a fourth-order polynomial, obtained from a least-squares fit in the spectral regions in which no significant cometary emission signal is apparent (namely, by excluding the regions 2.55 to 2.85, 3.20 to 3.50 and 4.10 to 4.40 μm; we checked that other choices did not significantly affect the spectra).

An additional interference is also occasionally present in the spectral region 4 to 5 μm. It consists of a small periodic ripple, tentatively attributed to vibrations of the filter wheel. It has been removed by Fourier filtering.

The last step of data processing is to convert the spectral intensity scale into physical units by applying the wavelength-dependent instrumental transmission and detector sensitivity functions measured during the preflight calibration (Fig. 4e).

The last steps of the instrumental background removal procedure also eliminate any possible continuum cometary signal. So any information about dust continuum emission is lost. Broad molecular emission, as well as possible ice absorption features or broad dust emission features, but not narrow molecular bands, may also be affected by the polynomial baseline subtraction. Thus it is clear that the accuracy and reliability of the processed spectra are limited by the background signal removal procedure rather than by the sensitivity of the experiment.

3.2. Results

Figure 5 shows the average of the last five useful spectra of the preencounter sequence, obtained at $D \sim 40{,}000$ km. They were processed as explained in the previous section, and the reference spectra were taken at $D_0 \sim 200{,}000$ km. As was already found from the quick-look analysis (Combes *et al.* 1986a), three molecular spectral features are clearly present: the 2.7-μm band of H_2O, the ν_3 band of CO_2 at 4.25 μm, and a broader feature in the region 3.2–3.5 μm, which corresponds to the characteristic wavelength of the stretching mode of the CH group in hydrocarbons. But several other weaker features are also present: especially at the wavelength of the blend of the ν_1 and ν_5 bands of H_2CO (3.6

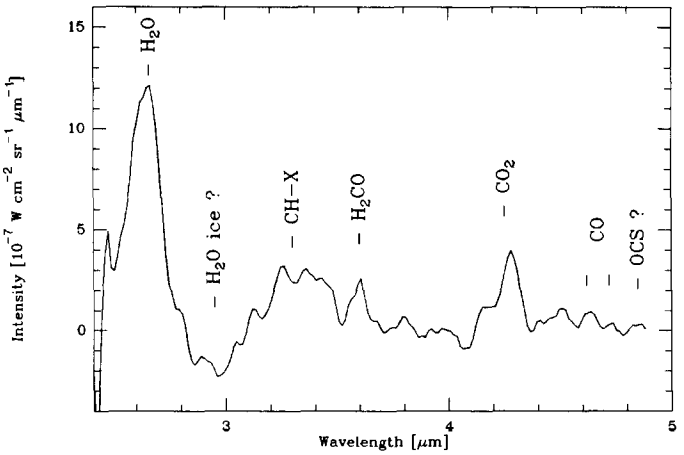

FIG. 5. The spectrum of comet Halley between 2.5 and 5 μm, obtained from the average of five individual spectra taken at $\langle D \rangle \sim 42{,}000$ km. The reference spectra are taken at $\langle D_0 \rangle \sim 200{,}000$ km and the reduction procedure is explained in Section 3.1. Possible molecular identifications are indicated.

μm), the 1 − 0 band of CO (4.7 μm), and an unidentified feature at 4.15 μm; possible absorption around 3.0 μm is also conspicuous. Whether these features are of cometary origin or are spurious and due to residuals of the background signal is a problem that should now be addressed.

3.2.1. Evolution of the Signal with the Probe–comet Distance

A powerful way to check the reality of such features is to study their variation as a function of the spacecraft–comet distance D. Parent molecules isotropically ejected from the nucleus with constant expansion velocity have a density proportional to r^{-2} (r being the distance to nucleus). Thus, any emission mechanism that has intensity proportional to the molecular density will give a signal proportional to D^{-1}. Therefore, if the observed spectral features indeed come from parent molecules, one should expect to find, at least in the first order of approximation, a proportionality between their intensity W_i and the parameter

$$X_i = 1/D_i - 1/D_0$$

D_i being the spacecraft–comet distance at which spectrum S_i was obtained, and D_0 that at which the reference spectra were taken.

In fact, the signal evolution could depart from the D^{-1} law for several reasons:

1. Both observations (e.g., Lämmerzahl *et al.* 1986) and theory (e.g., Bockelée-Morvan and Crovisier 1987b) suggest that the expansion velocity is not constant, but slightly accelerating with increasing distance from the nucleus. This effect, which is not very important (the velocity increases by ~20% between $r = 2000$ and 20,000 km), would lead to a steeper law.

2. Some short-lived species might have a smaller scale-length than the instrumental field of view. This would also steepen the law. Among the species that will be considered below, however, this effect should be noticeable only for H_2CO, which has an expected scale-length of ~2000 km at 0.8 AU, to be compared with the 1700-km radius of the field of view at $D = 200{,}000$ km.

3. Some species might come not from the nucleus surface, but from distributed sources (e.g., from photosputtering of grains, from sublimating grains, or from gas-phase chemical processes). In this case, the law would be flatter, and these species might be undetectable. Indeed, it

was stated earlier (Crifo 1981, Crovisier and Encrenaz 1983) that the IKS instrument was not designed for the detection of daughter products.

4. Abundant species may have optically thick lines. This would lead to a flatter law, and necessitate a detailed radiative transfer treatment. This point will be discussed below for the H_2O and CO_2 features.

5. As shown by many observations, gas and dust are not ejected isotropically from the nucleus which is active only on restricted areas of the day side. "Jets" should be present in the near-nucleus region. However, the gas distribution should get more isotropic at large distances. Furthermore, the signal due to radial jets with a density proportional to r^{-2} should be proportional to D^{-1}, since the phase angle did not change significantly during the observing sequence.

6. The r^{-2} law of the gas density could be affected by temporal variations of the gas production rate.

With the exception of optical depth effects, all these effects should give only second-order modifications to the D variation of the signal of parent molecules. Indeed, *in situ* observations have revealed that the density of total neutral gas as well as that of some species agree with an r^{-2} law in the inner coma with a reasonable degree of approximation (Krankowsky *et al.* 1986, Curtis *et al.* 1986).

Figure 6 shows the evolution of the observed spectra as a function of D (or X). The spectra have been grouped and averaged for various bins of the distance. There is an obvious increase of the intensity of the spectral features at 2.8, 3.3, and 4.25 μm when the probe is approaching the comet, as expected for real cometary signals. To characterize this dependence better, we have fitted a regression

$$S(\lambda) = a(\lambda) + b(\lambda)X$$

for each spectral element $\Delta\lambda$ over the 103 corrected spectra that span most of the pre-

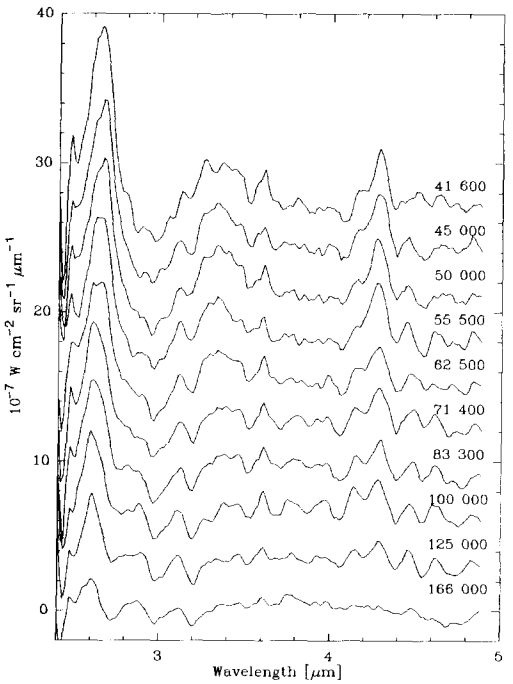

FIG. 6. Evolution of the spectra as a function of distance to nucleus. Spectra are grouped and averaged in bins according to the distance D to nucleus. The spectra are labeled on the right with their average distance in km. They have been shifted vertically relative to one another to avoid overlap. All the spectra are differences from a reference spectrum taken at $\langle D_0 \rangle \sim$ 200,000 km.

encounter observing sequence. The result is displayed in Fig. 7, which shows $b(\lambda)/D$ for D = 40,000 km, i.e., the "reconstructed spectrum" at 40,000 km from the comet. It is remarkable that this "spectrum" is close to the reduced spectrum obtained, for instance, close to the flyby and reproduced in Fig. 5. This strongly supports the hypothesis that most of the spectral features of the figure are of cometary origin. Also given in Fig. 7 are the formal errors resulting from the fit of the regression slope. One must note that these errors are not independent for adjacent spectral elements, and that one would not improve the signal-to-noise ratio by smoothing the spectrum. One must also note that, although they are indicative, these errors do not include the uncertainty due to the polynomial baseline removal.

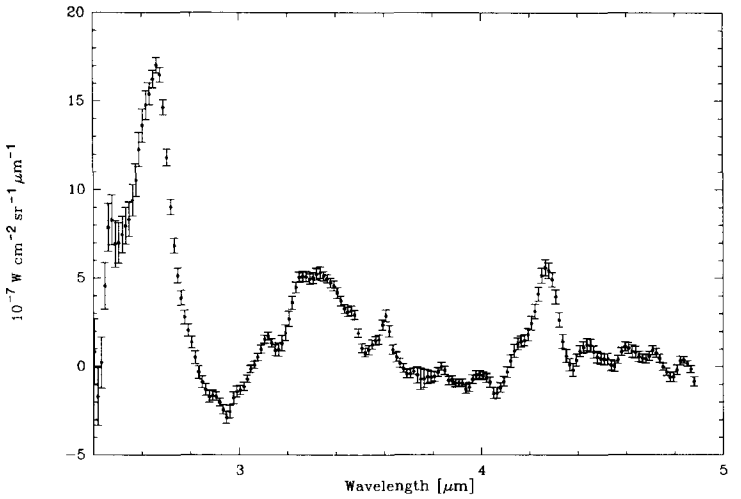

FIG. 7. The spectrum of comet Halley at D = 40,000 km resconstructed by extracting the part of the signal varying as D^{-1}. For this, a regression line $S(\lambda) = a + bX$ has been fitted to the set of spectra (see Section 3.2.1). The error bar is the 1σ formal error on the slope resulting from the fit.

For a more detailed study of individual molecular features, we present in Figs. 8a–e the evolution, as a function of X, of the signal

$$W = \int S(\lambda) d\lambda$$

integrated over the spectral ranges relevant to the detected or suspected molecular signatures. The results of the linear regression fits are shown in the figure and listed in Table II. We have also performed the same analysis when the spectra are grouped and averaged over 12 bins which ensure uniform coverage of the range of the X parameter, to exclude any possible bias due to the higher density of the data at small X's. The results, however, appear to be practically insensitive to this grouping.

When the shape of the molecular spectral feature is a priori known (e.g., from studies such as those of Crovisier 1987 or Bockelée-Morvan 1987), it is possible to use an adapted filtering analysis by just fitting the amplitude of the expected signal pattern to the observed spectrum. Such a fitting does not require the residual continuum to be removed by low-frequency filtering as explained in Section 3.1. This analysis was performed on the 2.7-μm H_2O feature and the 4.25-μm CO_2 feature, assuming bands of Gaussian shapes centered at the right wavelengths and with widths resulting from excitation models. The results are in excellent agreement with those of Figs. 8a and b and of Table II. This confirms that the signal is not significantly affected by the baseline determination. One should note that the adapted filtering method works very well for narrow isolated features, but cannot be applied to the 3.2–3.5 μm broad feature, for which no definite assignments have yet been made.

3.2.2. Production Rate Derivations

The integrated flux of the emission of a molecular band is

$$W = \frac{h\nu g Q}{4\pi\theta v_{\exp} D}$$

where Q is the molecular production rate (assumed to be isotropic), $v_{\exp}$ is the gas expansion velocity (assumed to be constant), θ is the full angular field of view, g is the emission rate per molecule. The lines are assumed to be optically thin. A full derivation of this formula was given by Crovi-

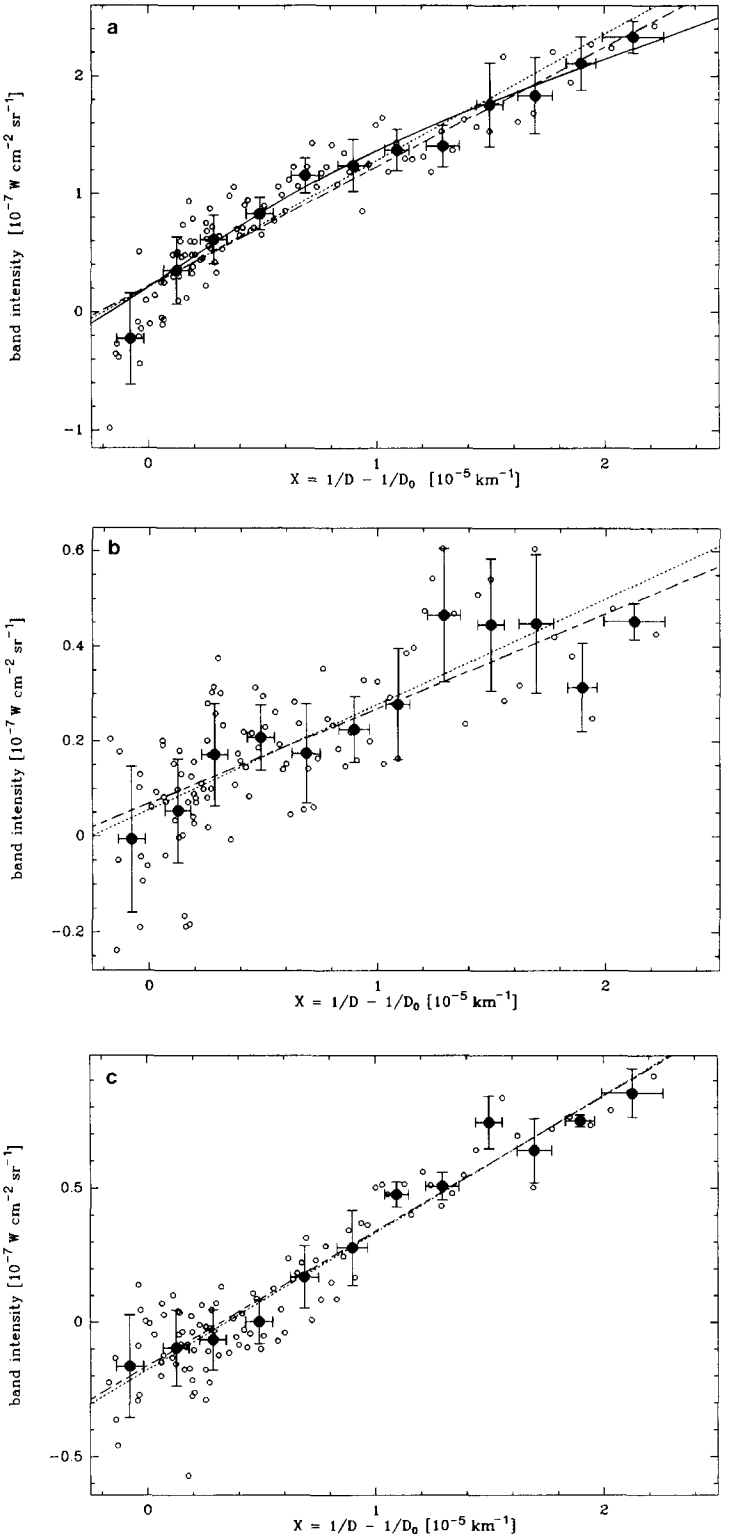
a
b
c
band intensity [10^{-7} W cm^{-2} sr^{-1}]
X = 1/D − 1/D$_0$ [10^{-5} km^{-1}]

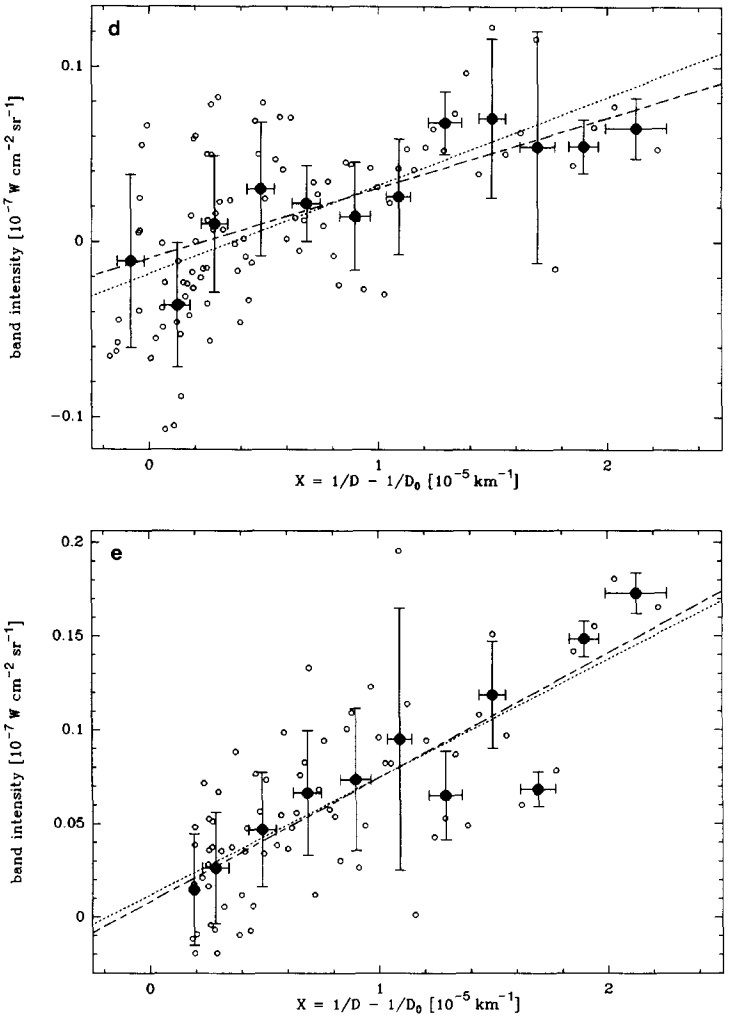

FIG. 8. Integrated line intensities W corresponding to several molecular features as a function of the parameter $X = 1/D - 1/D_0$. Unfilled circles correspond to individual spectra. Filled circles correspond to spectra grouped and averaged for various bins of the parameter X; the error bars indicate the dispersions of X and of intensity within the bin. For real cometary features, W is expected in first approximation to be proportional to X. The regression lines are drawn for both individual spectra (dotted lines) and grouped spectra (dashed lines). (a) H_2O; the full line corresponds to the expected law for $Q[H_2O] = 10^{28}$ sec^{-1} when line optical depth is taken into account. (b) CO_2. (c) CH–X. (d) CO. (e) H_2CO.

sier and Encrenaz (1983): it results from volume integration of the emission rate, the only approximation being that the linear field of view θD is supposed to be much smaller than the molecular scale-length. In the present case, W can be easily related to the slope b of the regression line fitted to W, so that

$$Q = \frac{4\pi v_{\exp} \theta b}{h\nu g}$$

We will assume here that $v_{\exp} = 0.8$ km sec^{-1}. This value agrees with that measured *in situ* at $r < 5000$ km (Lämmerzahl *et al.* 1986) and with those derived from the widths of the HCN radio lines (Bockelée-

Morvan *et al.* 1987, Schloerb *et al.* 1987). The emission rate, for resonant excitation by the Sun, is

$$g = B_{lu}J(\upsilon)$$

where the Sun radiation energy density $J(\nu)$ can be taken from Labs and Neckel (1968), and B_{lu} may be deduced from the laboratory-measured band strength S as explained by Crovisier and Encrenaz (1983).

The production rates (or their upper limits) obtained in this way are listed in Table II with the formal errors resulting from the regression fit. We will now proceed to separate discussions for each spectral feature.

3.2.3. The Water Band at 2.7 μm

This band is a blend of at least two fundamental (ν_1 and ν_3) and two combination ($\nu_2 + \nu_3 - \nu_2$ and $\nu_1 + \nu_3 - \nu_1$) vibrational bands, but the ν_3 band is expected to have the strongest emission rate (Crovisier 1984). Individual lines from the ν_3 band of water were previously detected in December 1985 in comet P/Halley from airborne observations (Mumma *et al.* 1986), directly revealing for the first time the presence of water in a comet.

The linearity of the signal as a function of X (Fig. 8a) is remarkable. This strongly suggests that most of the water is directly coming from the nuclear region (and not from a distributed source such as icy grains). This also shows that the water scale-length is larger than 5000 km, in agreement with the H_2O photodestruction theory (Huebner, 1985) and with the scale-length measured *in situ* (Krankowsky *et al.* 1986).

The water production rate cannot be evaluated using the linear formulas of Section 3.2.2, because the strong ν_3 band is optically thick in the region of the coma observed by the IKS instrument. The saturation effect has been estimated by Bockelée-Morvan and Crovisier (1986, 1987a) and Bockelée-Morvan (1987), treating the radiative transfer problem with the escape probability formalism, and solving simultaneously for the water rotational distribution. A similar approach was made by Bisikalo *et al.* (1987). Krasnopolsky and Tkachuk (1987) also estimated the band sat-

TABLE II

ASSIGNMENTS OF OBSERVED FEATURES AND MOLECULAR PRODUCTION RATES

Molecular band		Wavenumber (cm^{-1})	Emission rate[a] (sec^{-1})	Integration range[b] (μm)	Regression coefficient[c]	Slope b[d] (W cm^{-1} sr^{-1})	Production rate (sec^{-1})
H_2O	ν_3	3756	2.8×10^{-4}	2.55–2.85	0.916	1070 ± 46	$4.5 \pm 0.2 \times 10^{29}$[e]
	ν_1	3657	3.2×10^{-5}				$1.0 \pm 0.1 \times 10^{30}$[f]
	$\nu_2 + \nu_3 - \nu_2$	3756	2.3×10^{-5}				
	$\nu_1 + \nu_3 - \nu_1$	3657	1.9×10^{-5}				
CO_2	ν_3	2349	2.9×10^{-3}	4.20–4.37	0.717	222 ± 21	$1.8 \pm 0.2 \times 10^{28}$[e]
							$2.7 \pm 0.3 \times 10^{28}$[f]
CH–X	C–H stretch	~3000	1.3×10^{-4}[g]	3.20–3.52	0.911	510 ± 23	$\sim 9.0 \pm 0.4 \times 10^{29}$[h]
CO	(1–0)	2143	2.6×10^{-4}	4.57–4.78	0.584	51 ± 07	$5.0 \pm 0.7 \times 10^{28}$
H_2CO	ν_1	2782	2.6×10^{-4}	3.52–3.65	0.683	63 ± 08	$4.0 \pm 0.5 \times 10^{28}$
	ν_5	2843	3.2×10^{-4}				
OCS ?	ν_1	2062	3.0×10^{-3}	4.79–4.88	0.257	43 ± 16	$< 7 \times 10^{27}$

[a] Theoretical fluorescence rate in the optically thin case for solar excitation at 1 AU.
[b] Wavelength integration range for the regression line analysis.
[c] Regression coefficient for the linear regression analysis of individual spectra.
[d] Slope of the regression $W = a + bX$, where $W = \int S(\lambda)d\lambda$, $X = 1/D - 1/D_0$, and $D_0 = 200{,}000$ km.
[e] For the optically thin case.
[f] Corrected for optical thickness (see text).
[g] Average value for a C–H stretch (see Sect. 3.2.5).
[h] $\Sigma nQ[C_nH_m]$ assuming gas-phase fluorescence (see Sect. 3.2.5).

uration by using a single scattering approximation and assuming a thermal rotational distribution for water. The results lead to an estimation of $Q[H_2O] = 10^{30}$ sec^{-1}; at $D = 40{,}000$ km, the ν_3 band is attenuated by a factor of ~3.5, whereas the other bands, which are much weaker, are practically unaffected (Bockelée-Morvan and Crovisier 1987a). A consequence of the optical depth effect is that the signal is no longer proportional to D^{-1} and should depart from a linear law in Fig. 8a. Therefore, the shape of the observed signal variation could in principle lead to a test of the saturation effect. The signal variation expected from the model is represented as a full line in Fig. 8a. It is indeed in overall agreement with the observations, but the accuracy of the latter is not sufficient to discriminate between a linear variation and the predicted law and to allow us to test the water excitation model. However, a more extreme saturation, which would lead to a larger curvature, seems to be excluded.

To our knowledge, the only other determination of the water production rate at the moment of the VEGA 1 encounter is 1.4×10^{30} sec^{-1}, derived from the observation of H and O by the Pioneer Venus ultraviolet spectrometer (Stewart 1987). Measurements made a few days later by the VEGA 2 (9 March) and Giotto (14 March) probes lead to consistent evaluations, when the variations of the comet activity are taken into account (at these moments, the comet was less active than on March 6): on VEGA 2, the three-channel spectrometer TKS measured a water production rate of 8×10^{29} sec^{-1} from its 1.38-μm band (Krasnopolsky *et al.* 1986), and an OH-parent production rate of 9×10^{29} sec^{-1} from the 310-nm OH band (Moreels *et al.* 1986); on Giotto, the neutral mass spectrometer NMS measured $Q[H_2O] = 5.5 \times 10^{29}$ sec^{-1}. Ultraviolet observations by IUE (Festou *et al.* 1986) lead to water production rates of 5.6×10^{29} and 5.2×10^{29} sec^{-1} at the times of the VEGA 2 and Giotto flybys, respectively.

At the moment of the VEGA 1 flyby, the total neutral gas production rate was evaluated as 1.3×10^{30} sec^{-1} by the PLASMAG-1 experiment (Gringauz *et al.* 1986) and 10^{30} sec^{-1} by the NGE experiment (Curtis et al. 1986). Compared with our H_2O production rate determination, this confirms that water is the dominant volatile product of the cometary nucleus.

3.2.4. The ν_3 Band of Carbon Dioxide at 4.25 μm

The 4.25-μm feature (Fig. 5), which we attribute to the ν_3 band of carbon dioxide (Fig. 9), is the first direct detection of this molecule in a comet. The linear dependence of the signal as a function of X (Fig. 8b) is clear. However, it is not as accurately defined as for H_2O. We note the presence of a spurious feature in the wing of the band at 4.13 μm, which does not show any variation with distance from the nucleus. As for H_2O (Sect. 3.2.3), the determination of the CO_2 production rate from its strong ν_3 band intensity needs a correction for optical depth. The saturation of this band amounts to a factor of 1.5 at $D = 40{,}000$ km (Bockelée-Morvan and Crovisier 1987a). The resulting production rate is 2.7×10^{28} sec^{-1}.

The presence of CO_2 in comets was suspected well before the VEGA flyby because of the presence of CO_2^+ bands in the ion tails. However, no reliable determination of $Q[CO_2]$ could be derived from the observation of these bands. The neutral mass spectrometer on Giotto measured a volume mixing ratio of 3.5% for the mass 44 relative to water (Krankowsky *et al.* 1986). This can be considered as an upper limit to $Q[CO_2]/Q[H_2O]$, since other molecules such as CS and C_3H_8 could also contribute to mass 44. This limit is in agreement with our determination.

Carbon dioxide is thus an important secondary constituent of cometary nuclei. CO_2 is much more volatile than H_2O, and could play an important role in the activity of comets at large heliocentric distances. As proposed by Feldman et al. (1986), it could

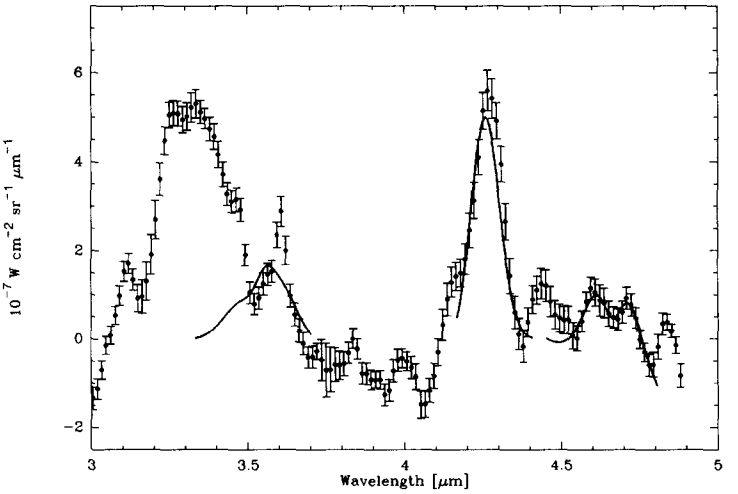

FIG. 9. Reconstructed spectrum between 3 and 5 μm (from Fig. 7), with superimposed synthetic band profiles of H_2CO, CO_2, and CO (a linear baseline has been added to the CO profile).

also be responsible for cometary outbursts at shorter heliocentric distances.

3.2.5. The 3.2- to 3.5-μm Feature

The intensity of this feature has a very well defined linear dependence with X (Fig. 8c), characteristic of an r^{-2} density law for the species responsible for this emission. This feature is too broad to be the signature of a single gaseous species. Therefore, it should arise from a mixture of many simple molecules, or from complex polyatomic molecules, or from dust particles. The wavelength of the feature is characteristic of the vibration of the C–H bond.

After the first report of the presence of this feature in the spectrum of comet Halley (Combes *et al.* 1986a), its detection was confirmed by ground-based observations (Baas *et al.* 1986, Danks *et al.* 1987, Knacke *et al.* 1986, Wickramasinghe *et al.* 1986). This feature is apparently transient, since it was not present in spectra of comet Halley taken at the end of 1985 (Danks *et al.* 1987). Such a feature was not present in the spectrum of comet West 1976 VI (Oishi *et al.* 1978) nor in comet IRAS-Araki-Alcock 1983 VI (Hanner *et al.* 1985), but was recently detected in comet Wilson 1986l (Brooke *et al.* 1987, Allen and Wickramasinghe 1987).

The 3.2–3.5 μm feature, which appears as a broad and mainly structureless emission in the present study, has been resolved into two distinct emission features at 3.28 and 3.37 μm by several ground-based observations, in particular those of Baas *et al.* (1986).

Three different origins have been invoked to explain this feature in P/Halley:

1. Heating of very small organic grains, or large polycyclic aromatic hydrocarbon molecules (PAH) by individual UV photons, in analogy with what is observed in the interstellar medium (see, e.g., Sellgren 1984, Léger and Puget 1984).

2. Thermal emission by small cometary grains with organic mantles, such as the "CHON" particles observed by the space-probes (Kissel *et al.* 1986a,b), which could be comparable to the organic residues observed in the laboratory from the irradiation of ices.

3. Resonant fluorescence of small gaseous molecules by the infrared radiation

field (ultraviolet excitation can be ruled out, since for simple stable molecules, it leads to dissociation rather than fluorescence).

The first mechanism has been suggested by Baas *et al.* (1986) in analogy with the excitation mechanism observed in the vicinity of UV sources. It can account for the 3.28-μm component of the cometary emission.

The second mechanism has been suggested by Knacke *et al.* (1986). Spectra of organic residues produced by laboratory irradiation of ices have been recorded by Chiba and Sagan (1987) in the region 2–20 μm. Models of thermal emission by cometary grains have been performed by Krishna Swamy *et al.* (1988) and Chiba and Sagan (1987). According to these studies, we would expect in P/Halley's spectrum weak emission features in the region 6–9 μm, which could show up by a few percent above the blackbody and silicate continuum. Apparently these features are not present (see Sect. 4.2.1), but the signal-to-noise ratio of the available data is not really sufficient to make this test unambiguous. The presence of the cometary emission at 3.28 μm, which does not appear in the laboratory spectra of organic residues, is more difficult to interpret with this mechanism than with the preceding one.

The third mechanism has been considered in our previous studies (Combes *et al.* 1986a–d, Moroz *et al.* 1987a,b) and by Knacke *et al.* (1986) and Danks *et al.* (1987). Resonant fluorescence of gas molecules, which is also responsible for all the other emissions observed in the range 2.5–5 μm (Sect. 3.2), also accounts for the absence of associated features at 7.7 μm, since the other vibrational bands of these species in the range 6–12 μm (bending modes) are not expected to yield detectable signatures (Crovisier and Encrenaz 1983). It could also explain the double structure emissions at 3.28 and 3.37 μm assessed by ground-based observations.

In the absence of unambiguous discrimination between the processes described above, we will estimate below the carbon abundances implied in the cases of (a) emission by PAH or grains and (b) fluorescence of gaseous molecules.

Emission by PAH or small cometary grains. The carbon abundance inferred from the 3.3-μm emission, in the case of thermal emission of small grains, can be estimated following Knacke *et al.* (1986) and Brooke and Knacke (1987). For a temperature of 500 K (which is the expected temperature for 0.1-μm particles), we derive $Q[C] \sim 3.2 \times 10^{27}$ sec^{-1} (Encrenaz *et al.* 1988), i.e., about 1% of the H_2O production rate. In the case of heating of PAH by transient UV photons, the carbon required to account for the observed emission is even smaller: the number of "large molecules" would be only 0.05% if, following Baas *et al.* (1986), one assumes a g factor of 0.2 sec^{-1} for 3.3-μm emission at 1 AU. The corresponding carbon amount is thus less than 1% of H_2O.

Following this scenario, the total carbon amount found in both the solid phase (3.2–3.5 μm emission) and the gaseous phase (CO, CO_2, H_2CO fluorescence) is only about 15% of H_2O. Taking into account other possible depositories of oxygen (gases and silicates), this leads to a cometary abundance ratio of $[C]/[O] \sim 0.10$, as discussed in more detail by Encrenaz *et al.* (1987, 1988). When compared with the cosmic abundance of carbon ($[C]/[O] \sim 0.5$), this suggests that more than 80% of the carbon would have to be in cometary grains, in the form of amorphous carbon or of large grains, which would not be detectable in the infrared.

Emission due to gaseous fluorescence. The 3.3–3.5 μm emission cannot be due to the ν_3 band of CH_4 alone, which would fall just between the two peaks, but could be due to a large number of hydrocarbons, as indicated in the compilation shown in Fig. 10 and Table III, and discussed by Grigoriev (1987). Instead of trying to determine the abundance of a given hydrocarbon mol-

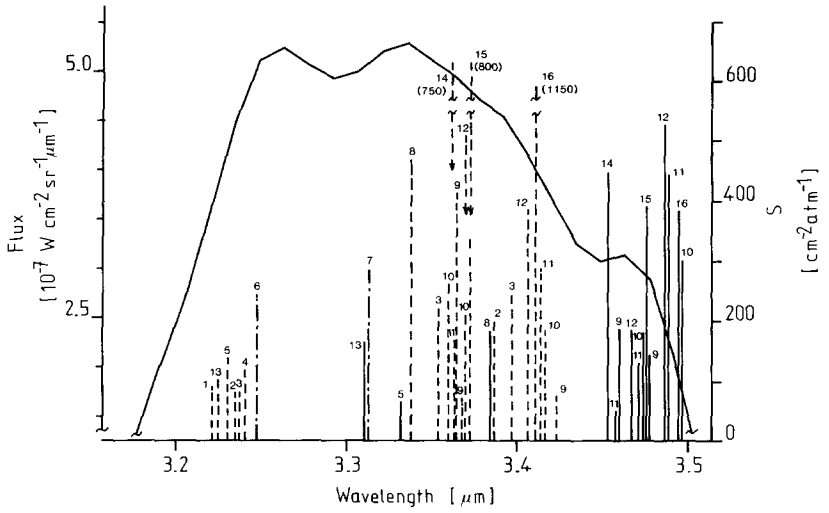

FIG. 10. Reconstructed spectrum of the emission feature 3.2–3.5 μm (from Fig. 7), with the relative band strengths S of several saturated and unsaturated hydrocarbons. The band strengths are compiled from Sverdlov *et al.* (1970). The code to the various molecules is given in Table III. See Grigoriev (1987). Solid lines: symmetrical stretching of [C–H] in CH_2 and CH_3. Dashed lines: antisymmetrical stretching of [C–H]. Dashed–dotted lines: other modes.

ecule, we will estimate the carbon amount in a given class of hydrocarbons. Figure 10 and Table III show that the 3.4-μm signature is characteristic of the C–H stretch in saturated hydrocarbons (alkanes), while the 3.3-μm signature can be produced by unsaturated hydrocarbons (alkenes, alkynes, aromatics . . . ; see also Bellamy 1975). The band strength is well known for alkanes (Finkel 1966); as a typical value, we adopt $S = 150$ cm^{-2} atm^{-1} per C–H stretch (i.e., per H atom). There is a larger uncertainty for the strength of the 3.3-μm bands of unsaturated hydrocarbons; by analogy

TABLE III

CODE TO MOLECULES IN FIG. 10

1 $H_2C{=}CH_2$	12 $CH_3{-}CH_2{-}CH_2{-}CH_2{-}CH_2{-}CH_3$
2 $H_3C{-}CH{=}CH_2$	13 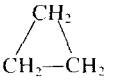
3 $(CH_3)_2{=}C{=}CH_2$	
4 $H_2C{=}C{=}CH_2$	14 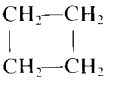
5 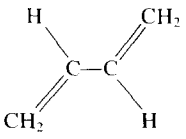	15 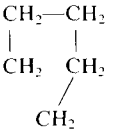
6 	16 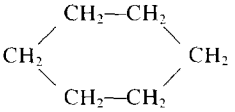
7 CH_4	
8 $CH_3{-}CH_3$	
9 $CH_3{-}CH_2{-}CH_3$	
10 $CH_3{-}CH_2{-}CH_2{-}CH_3$	
11 $CH_3{-}CH_2{-}CH_2{-}CH_2{-}CH_3$	

with the value measured for aromatic compounds (d'Hendecourt and Allamandola 1986, Léger and d'Hendecourt 1987) we adopt $S = 50$ cm^{-2} atm^{-1} per C–H stretch (i.e., per H atom). The IKS data do not allow us to separate the saturated and unsaturated components; however, we know from ground-based observations (Baas *et al.* 1986, Danks *et al.* 1987) that the flux in the 3.3-μm feature is about a third of the 3.4-μm flux. We can thus assume that saturated and unsaturated hydrocarbons are in comparable amounts, and assume for the whole feature a "mean" strength of 100 cm^{-2} atm^{-1} per C–H stretch, which corresponds to an emission rate $g = 1.3 \times 10^{-4}$ sec^{-1} at 1 AU. Then the derived production rate of C–H stretches deduced from the IKS observation (Table II) is $\sim 7 \times 10^{29}$ sec^{-1}.

To derive a production rate for carbon atoms present in hydrocarbons, we need to know the extent of saturation of each hydrocarbon class. In the case of alkanes, we have C/C–H = 0.5; for unsaturated hydrocarbons, the numbers are more uncertain, but we can reasonably assume C/C–H = 2, from observed spectra of organic residues (d'Hendecourt, private communication). Then, the rates of production of carbon atoms are $\sim 2 \times 10^{29}$ sec^{-1} in saturated hydrocarbons and $\sim 7 \times 10^{29}$ sec^{-1} in unsaturated hydrocarbons, thus a total of 90% of the number of water molecules.

Since the photodissociation process of gaseous hydrocarbons should result in the production of nearly one CH radical per C atom (at least for the saturated form), it is interesting to compare the carbon production rate deduced above with the CH-radical production rate inferred from the observation of the CH bands in the visible. Unfortunately, this is still a debated question, because the CH lifetime is poorly known. Assuming a CH lifetime of ~100 sec, Krasnopolsky *et al.* (1986) estimated $Q[\mathrm{CH}]/Q[\mathrm{H_2O}] \sim 0.10$ from the VEGA 2 measurements. From ground-based observations, Wyckoff *et al.* (1988) estimated the CH lifetime to be much larger (~5000 sec) and found $Q[\mathrm{CH}]/Q[\mathrm{H_2O}] \sim 0.007$. However, the recent calculations of Singh and Dalgarno (1987) confirm that the CH lifetime should be indeed around 100 sec, which leads to a reevaluation of the CH production rate from the observations of Wyckoff *et al.* close to our value for the production rate of carbon in saturated hydrocarbons, thus supporting the gaseous origin of the 3.2–3.5 μm feature, or at least part of it.

The abundance of carbon derived from the 3.2–3.5 μm feature, under the assumption of fluorescence excitation, is very large compared with the other sources of gaseous carbon; this result actually conflicts with the value of C/O expected from the cosmic abundances. More probably, the 3.2–3.5 μm cometary emission is due to a mixture of hydrocarbons in both solid and gaseous phases: part of the molecules in the organic mantles of grains is expected to sublimate when these latter are heated up to 500 K.

3.2.6. The $v(1 - 0)$ Band of Carbon Monoxide

The $v(1 - 0)$ band of CO at 4.65 μm is probably present at the limit of detection in the IKS spectra (Figs. 5, 7): the intensity variation of the feature as a function of distance is consistent with a D^{-1} law, but is fairly noisy (Fig. 8d and Table II) and less clear than for the H_2O, CO_2, or CH–X features. The feature is apparently double with peaks at 4.60 and 4.17 μm, which suggests that the P and R branches are resolved. In fact, the spectral resolution of IKS around 4.5 μm is $\Delta\lambda/\lambda \sim 1/70$, and the calculation of synthetic spectra (see Fig. 9 and Crovisier, 1987) shows that these branches should be resolved at such a resolution if the kinetic temperature of the coma is at least 100–150 K in the region sampled by the instrument. The production rate derived for CO is 5×10^{28} sec^{-1}, assuming a parent molecule spatial distribution.

Carbon monoxide is known to be a major constituent of comets since its observation in the UV in comet West 1976 VI with an

abundance $Q[CO]/Q[H_2O] \sim 0.2$. Its abundance, however, seems to be highly variable from comet to comet. For comet Halley, UV observations yielded CO abundances of 10–20% from IUE observations (Festou *et al.* 1986), of 17 ± 4% from rocket observations (Woods *et al.* 1986), both at the moment of the spacecraft encounters. *In situ* measurements with the neutral mass spectrometer NMS aboard Giotto suggested that a large fraction of the CO does not come directly from the nucleus, but from another source in a distributed region at $1000 < r < 20{,}000$ km (Eberhardt *et al.* 1987); the NMS measurements lead to a total CO production rate in agreement with the UV observations, but they indicate $Q[CO]/Q[H_2O] < 0.07$ for the fraction directly coming from the nucleus. This is consistent with our observations (even if our CO production rate is interpreted as an upper limit), which were not sensitive to the fraction of CO coming from the distributed source.

3.2.7. *The ν_1 and ν_5 Bands of Formaldehyde*

A narrow feature is apparent at 3.59 μm in the IKS spectrum (Fig. 5). Its intensity apparently follows the D^{-1} law expected for parent molecules (Fig. 8e), although less clearly than for the H_2O, CO_2, and CH–X species. A possible identification is formaldehyde, which has its two fundamental bands ν_1 and ν_5, of nearly equal strength, at central wavelengths of 3.59 and 3.52 μm, respectively. Figure 9 shows the expected emission profile of the blend of ν_1 and ν_5 (other combination and harmonic bands of H_2CO in the same spectral range are estimated to have negligible fluorescence emission with respect to these fundamental bands). This profile is computed for a thermal rotational population at 300 K, from the GEISA spectroscopic data bank (Husson *et al.* 1986). The A-type ν_1 band is relatively narrow, whereas the B-type ν_5 band is broad. At the spectroscopic resolution of IKS, a single peak is resulting at a wavelength of 3.56 μm, near the observed feature. Thus the identification seems reliable. Note that the observed spectrum (Fig. 7) shows a narrow spike affecting three spectral elements at 3.60 μm; this spike, which is narrower than the instrumental resolution, is not related to the molecular band structure.

The signal intensity listed in Table II corresponds to the spectral range 3.52 to 3.68 μm. We estimate that it includes all the ν_1 band, and half the ν_5 band energy. The resulting production rate for H_2CO is 4×10^{28} sec^{-1} in the case of resonant fluorescence. But since this spectral range might also be contaminated by some of the CH-bearing products responsible for the 3.2–3.5 μm broad feature, and since electronic excitation at visible wavelengths could also contribute to fluorescence of the ν_1 and ν_5 bands, the real H_2CO production rate may be lower.

The ν_1 and ν_5 bands of H_2CO seem to be marginally present in some of the infrared spectra of P/Halley taken from the ground (Knacke *et al.* 1986, Danks *et al.* 1987), but not in other ones which, however, revealed the 3.2–3.5 μm feature (Baas *et al.* 1986, Wickramasinghe and Allen, 1986). This might be due to the short scale-length of H_2CO (~2000 km), smaller than the field of view of ground-based instruments. Formaldehyde was also detected in P/Halley through its 1_{10}–1_{11} rotational line at 4.8 GHz, with an abundance comparable to that observed by IKS (Snyder *et al.* 1988).

Formaldehyde is known to be present in interstellar dark clouds with abundances comparable to that of HCN. It has often been proposed as a major constituent of cometary nuclei. It is interesting to note that a periodic series of peaks observed by the heavy-ion mass spectrometer aboard Giotto has been interpreted as the signature of the decay products of polyoxymethylene, which is polymerized formaldehyde (Mitchell *et al.* 1987, Huebner 1987, Huebner *et al.* 1987). However, formaldehyde observed by IKS, which has a parent mole-

cule distribution, should come from the nuclear region and not from the progressive unzippering of polyoxymethylene. The main photodissociation pathway of H_2CO leads to the release of CO (Huebner 1985). Thus, formaldehyde could be in part the other source of CO which seems to be needed to explain the difference between the CO production rates obtained from the UV observations (Festou *et al.* 1986, Woods *et al.* 1986) and from the present experiment (Sect. 3.2.6).

3.2.8. The Region 2.8–3.15 μm

The region that extends between the 2.7-μm bands of water and the 3.2–3.5 μm broad emission feature possibly shows broad absorption around 3 μm, narrow emission at 3.10 μm, and perhaps emission around 2.8 μm in the wing of the water band (Figs. 5, 6, 7). As previously noted in Section 3.1, the reliability of the broad absorption feature is hampered by the polynomial baseline removal used in the data processing. The absorption at 2.9 μm shown in Fig. 7 amounts to about 10% of continuum (the latter being evaluated from the 3.45-μm photometric observation of March 6.85 by Hanner *et al.* 1987, scaled to the IKS instrument assuming the continuum intensity to be proportional to the field of view). This spectral region is characteristic of the O–H bond stretching mode. Several coma constituents are expected to have signatures in this range.

1. The broad absorption at 2.8–3.0 μm and the narrow emission feature at 3.12 μm are very similar to the expected signature of water–ice grains: see, for instance, the spectral profiles computed by Hanner (1984) and by Crifo and Emerich (1985). Since the scale-length and the temperature of volatile grains are both much smaller than those of refractories, any ice signature should be presumably weak. Crifo and Emerich (1985) have made a model computation of the signals expected for the IKS instrument if, in addition to the standard comet Halley encounter model, one assumes 20% of the water production under the form of icy grains. Scaling their results to the measured water production rate, one predicts in the 3-μm region a continuum flux from this icy halo of $\sim 4 \times 10^{-7}$ W cm^{-2} sr^{-1} μm^{-1} if the ice is pure, and about a factor of 10 less if the ice is impure. These numbers are orders of magnitude only, being dependent on the initial icy grain size. Comparing with Fig. 5, one sees that the possibility of observing an ice emission is indeed open.

2. Water clusters are expected to form in the coma following the strong expansion cooling of water (Kitamura and Yamamoto 1986, Crifo, 1987, 1988a). The larger clusters will scatter solar light like tiny ice crystals, and in addition, the smaller clusters (dimers, etc.) have an important predissociative absorption band in the region 2.7–3.0 μm (Coker *et al.* 1985), and could contribute to absorption in this spectral range. Detailed modeling of the cluster emission (Crifo 1987) indicates that the signal seen by the IKS instrument near 3 μm due to the clusters does not exceed 10^{-14} W cm^{-2} sr^{-1} μm^{-1} and is therefore negligible. An exact computation of the absorption by predissociation of small clusters is not possible because of the lack of relevant cross sections. However, Crifo (1988a) has shown that their abundance relative to water is everywhere less than 1%, and even less than 10^{-5} in most of the water coma. Accordingly, observations of absorption features from water clusters is also unlikely.

3. The emission around 2.8 μm does not show any clear dependence on D. It shows up clearly only in the spectra taken at $60{,}000 < D < 150{,}000$ km (Fig. 6). It is indeed difficult to isolate this feature, due to the presence of the much stronger H_2O bands, and the contamination by instrumental emission ("b" component, Sect. 3.1). The presence of emission at 2.8 μm was also subsequently observed from the ground in P/Halley by Tokunaga *et al.* (1987) and in comet Wilson 1986l by Brooke *et al.* (1987). Such an emission could be due

to the OH $v(1 - 0)$ band, which has its Q branch centered at 2.80 μm. The fluorescence of OH vibrational bands, however, cannot yield significant signal (Crovisier and Encrenaz 1983), and another emission mechanism should be invoked. It is possible that the photodissociation of water produces OH in excited states of vibration. Indeed, several bands of the sequence $\Delta v = 2$ of OH were observed in the near-infrared spectrum of P/Halley (Krasnopolsky *et al.* 1986). Laboratory measurements (Andresen *et al.* 1984) have shown that the photodissociation of H_2O at 157 nm yields more than 53% of OH in excited vibrational states. Assuming that the yield of $v(1 - 0)$ OH emission subsequent to water dissociation is 50%, we infer an emission rate $g = 6 \times 10^{-6}$ sec^{-1} per water molecule at 1 AU for this band, to be compared with $g = 3.3 \times 10^{-4}$ sec^{-1} for the 2.7-μm water bands in the optically thin case. Thus we expect an OH signal approximately one-fiftieth that of the water band (which is consistent with that observed by Tokunaga *et al.* 1987), which can be seen against water emission in the IKS spectrum only with considerable difficulty.

3.2.9. Other Possible Features

Several other spectral features may be suspected just above the noise level, at 3.85, 4.0, 4.45, and 4.85 μm. We have checked that they are not due to the periodic ripple occasionally present in the region 4–5 μm (Sect. 3.1). Admittedly, these features are not firm detections, but it is nevertheless interesting to discuss their possible identification and to infer the constraints on the abundances of the relevant molecular species.

The 4.85-μm feature is the most promising one, because it coincides with the strong ν_1 band of OCS. The feature intensity corresponds to a production rate of 7×10^{27} sec^{-1}, which may be considered as a 2.5σ detection or an upper limit. Therefore the OCS abundance is less than 0.01 that of water (an upper limit of 0.06 was obtained from radio observations by Bockelée-Morvan *et al.* 1987). The production rates of sulfur in S_2 and CS molecules are on the order of 10^{-3} $Q[H_2O]$, but that of atomic sulfur is ~ 0.02 $Q[H_2O]$, according to Azoulay and Festou (1986). This suggests that cometary sulfur is deposited in parent molecules other than S_2, CS_2, or OCS, or in grains.

The other features are less interesting, because they can be assigned only to weak bands or combination bands, and therefore they do not lead to significant upper limits on molecular production rates. The 4.45-μm feature is close to the C≡N stretching mode; for instance, the ν_2 band of HC_3N is at 4.40 μm, but the feature intensity would correspond to an unrealistic production rate (2×10^{29} sec^{-1}, which is much larger than the upper limit deduced from the observations at radio wavelengths of Bockelée-Morvan *et al.* 1987). The 4.45-μm feature might also be the signature of C≡N bonds in small grains, but this signature is rather shifted toward 4.60 μm, as shown in laboratory spectra of organic residues (d'Hendecourt *et al.* 1986). The 3.8-μm feature is near the ν_1 band of H_2S, that of 4.0 μm near the $\nu_1 + \nu_3$ band of SO_2, but this also leads to meaningless production rates, because of the weakness of these bands.

4. THE SPECTRUM FROM 6 TO 12 μm

4.1 Data Processing

4.1.1. Elimination of the Background Signal

As in the case of the 2.5–5 μm channel, the raw spectra of the long-wavelength channel are dominated by the internal background signal. This effect is even stronger here, since the instrumental background emission that corresponds to a mean temperature of about 290 K peaks in the spectral interval 6–12 μm.

The data processing method used for the 6–12 μm channel is similar to the method described in Section 3.1 for the 2.5–5 μm channel. To first order, we make the differ-

ence between a current spectrum S_i and a reference spectrum S_R taken at the beginning of the observing sequence. As in the case of the SSC, there is still background remaining after this operation. This background consists of two components of the same nature as the components a and b found for the SSC:

(a) A component that varies slowly with the temperature variations of the instrument. This component can be reliably removed with the help of the accurate monitoring of the temperatures of the instrument during the observing sequence and the use of preflight calibration data.

(b) A modulation correlated with the fluctuation of the cryostat temperature. In the case of the SSC, this component is small compared with component a, and is limited to some wavelength intervals (mostly $\lambda < 3$ μm). In contrast, in the case of the LSC, this component (b) affects the whole spectral range and is about 50 times stronger in the 6–12 μm channel than in the 2.5–5 μm channel. We were not able to parameterize it accurately enough to perform a reliable correction, as was done for the SSC. As a consequence, we used only a very limited number of spectra (a dozen), sampled in six groups of two consecutive spectra each, over the whole observing sequence, for which the cryostat temperature had a constant value. This component (b) was actually responsible for the emission at 7.5 μm which was erroneously interpreted as a cometary signal in the preliminary report of the IKS results (Combes *et al.* 1986a).

4.1.2. Variation of the Signal as a Function of the Comet–Probe Distance

After having removed component a of the selected spectra as mentioned above, we were able to plot the residual signal as a function of nucleus distance (Fig. 11). As the cometary signal is expected to be due mostly to cometary dust, we could expect, if the dust is emitted at constant velocity from the nucleus, a D^{-1} variation. Instead of such a law, we observed a strong signal at the early beginning of the observing sequence ($D \sim 275{,}000$ km) which decreased rapidly down to a minimum value for $D \sim$

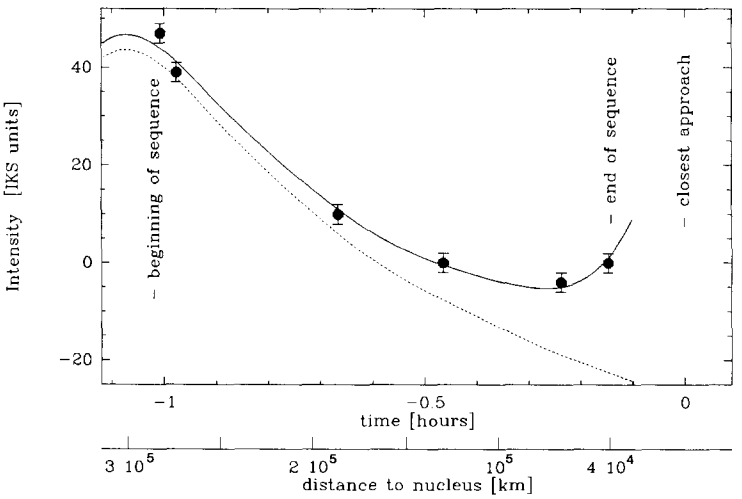

FIG. 11. Variations of the external signal measured at 10 μm by the instrument as a function of time and of the probe–nucleus distance (circles with error bars). The solid line is the result of a fit to a two-component model; the first component (dotted line) is due to instrumental emission and is assumed to be proportional to the temperature of the telescope spider (see Section 4.1.2); the second component is of cometary origin and is supposed to vary as D^{-1}.

70,000 km, and increased again from this distance up to the end of the sequence ($D \sim$ 40,000 km). The signal, which shows the general spectral shape of the instrumental transmission function, has to be of external origin. Its decrease at the beginning of the sequence can be interpreted as the variation of the temperature of the telescope spider, which is the only external part of the instrument (i.e., located beyond the filter wheel) that was in the field of view. Indeed, the shape of the spectrum corresponds to that of a blackbody at about 300 K. Moreover, the monitoring of the temperature of the spider shows a continuous decrease (Fig. 3). Figure 3 also shows that, even at distances to the nucleus shorter than 70,000 km, the spider temperature (as all other external temperatures) continued to decrease. Thus, the increase of residual signal observed in Fig. 11 cannot be due to the same origin. Since this signal, which still reflects the shape of the instrumental transmission function, has to be of external origin, we believe that it is of cometary origin.

To proceed further with the analysis, we have fitted to the observed signal the sum of a $1/D$ component (supposed to be the comet signal) and of a component varying linearly with the spider temperature. As shown in Fig. 11, such a two-component model fits the data very well. The zero level is not easily determined since, in the IKS instrument, only modulations of the signal as a function of wavelength were recorded. Therefore, we adjusted the zero level with reference to ground-based observations recorded at the same date (Hanner *et al.* 1987): since, outside the region 6–8 μm where silicate emission dominates, the ground-based spectrum is well represented by a 350 K blackbody, we have constrained our spectrum to fit this blackbody curve at 6 and 8 μm.

Figures 12a–c illustrate the different steps of the reduction. Figure 12a shows the cometary spectrum, obtained as the difference of two spectra recorded at distances D = 40,000 and 70,000 km, respectively, each spectrum being the average of two 18-sec consecutive scans, and after correction of component a and of the spider contribution (Fig. 11). Figure 12b is the transmission function, obtained from preflight calibration data. Figure 12c shows the ratio of the spectra of Figs. 12a and b, with an arbitrary intensity scale. This spectrum shows no strong narrow cometary features. However, some high-frequency periodical noise is present at $\lambda < 7.5$ μm. To improve the signal-to-noise ratio, high frequencies were filtered out. The resulting spectrum, which is shown in Fig. 13, has a resolving power of ~20.

Assuming the D^{-1} law for the variation of the signal, the total signal at D = 40,000 km is equal to 2.33 times the signal of the difference of spectra recorded at 40,000 and 70,000 km. We thus converted the scale of the cometary spectrum of Fig. 12a into absolute units, using preflight calibration data, and then multiplied this scale by the 2.33 factor. The resulting absolute scale is shown in Fig. 13, for a distance D = 40,000 km. The error bars shown in the figure take into account the noise of the data and the uncertainty in the zero-level definition. The accuracy of the absolute scale is believed to be about 20%.

4.2. Results and Interpretation

Several comments can be made on the spectrum shown in Fig. 13: (1) the spectrum shows no strong emission at 7.5 μm; (2) there are no narrow emissions between 6 and 11.6 μm; (3) the spectrum is dominated by a strong and broad feature with a double structure; (4) the absolute flux may be compared with that obtained by simultaneous ground-based observations.

4.2.1. Absence of 7.5-μm Emission

As mentioned above (Sect. 4.1.1), the feature that appeared at 7.5 μm in the preliminary reduction of the data (Combes *et al.* 1986a) was not of cometary origin, as

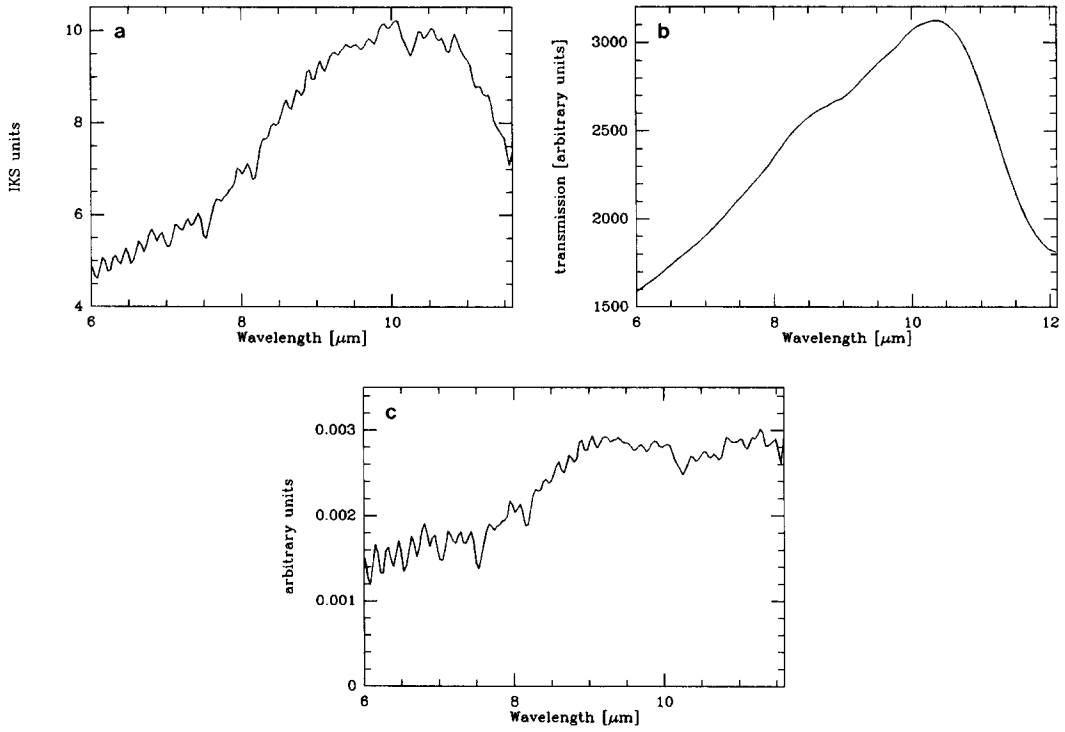

FIG. 12. Steps of the reduction of the spectrum of comet Halley between 6 and 11.6 μm. This spectrum is the difference of two spectra recorded at distances D from the nucleus of 40,000 and 70,000 km, respectively. Each spectrum is the sum of two consecutive scans of 18-sec integrating time each. (a) Spectrum before correction from the instrumental transmission. (b) Instrumental transmission function (arbitrary units). (c) Ratio of the raw cometary spectrum (a) to the transmission function (b) (arbitrary units).

erroneously stated by the authors, but was an instrumental effect. The final data (Fig. 13) show no emission at 7–8 μm. This was also reported from airborne observations (Campins *et al.* 1986, Bregman *et al.* 1987).

A weak emission might be marginally present at 6.8 μm. This marginal emission also appears in the KAO data of Bregman *et al.* (1987). The 6.8-μm wavelength corresponds to the vibration frequency of a C–H bond, especially CH_2 in saturated hydrocarbons. As noted by Bregman *et al.* (1987), it also corresponds to the signature of carbonates. This emission, if confirmed, cannot be due to resonant fluorescence at this wavelength (see Sects. 3.2.5 and 4.2.2). It might be attributed to the thermal emission by very small carbonaceous grains.

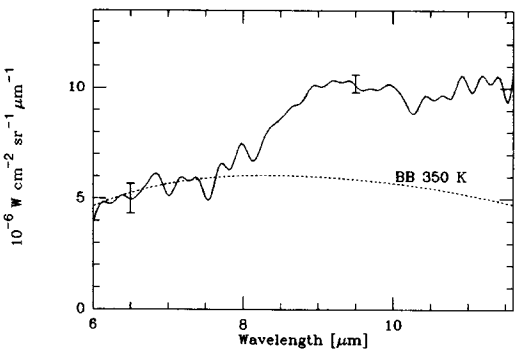

FIG. 13. Spectrum of P/Halley between 6 and 11.6 μm at a distance of 40,000 km from the nucleus. This spectrum results from that of Fig. 12c after smoothing and proper adjustment of the intensity scale (see Section 4.1.4). The 1° field of view corresponds to a diameter of 700 km centered on the comet's nucleus.

4.2.2. Absence of Narrow Molecular Emission Features

As shown in Figs. 12c and 13, there are no detectable molecular emission features in the 6–11.6 μm spectrum of comet Halley. From previous theoretical calculations (Crovisier and Encrenaz 1983), this result was not unexpected. Indeed, the resonant fluorescence excitation mechanism is not efficient beyond 5 μm, due to the rapid drop of the solar infrared flux at long wavelengths. The local IR dust radiation field is also too weak to lead to significant excitation. Even the ν_2 fundamental band of H_2O at 6.2 μm, which is the strongest gaseous emission expected in this spectral range, should be about three times weaker than the ν_3 band of H_2O at 2.7 μm. The integrated flux of the latter is 2×10^{-8} W cm^{-2} sr^{-1} at D = 40,000 km (see Sect. 3.2.3). The rms noise around 6 μm is about 6×10^{-9} W cm^{-2} sr^{-1} in a single spectral element ($\sim$0.03 μm), corresponding to a 3σ detection limit of 8×10^{-8} W cm^{-2} sr^{-1} for a 0.6-μm-wide feature. This is an order of magnitude larger than the expected integrated flux of the ν_2 band of H_2O.

4.2.3. The Silicate Emission

Figure 13 shows that the 6–12 μm spectrum of comet Halley is dominated by a very strong and broad emission between 8 and 12 μm. This feature had been previously recorded, on P/Halley as on several other comets, from ground-based photometric measurements (e.g., Hanner *et al.* 1987) and was identified as silicate emission; the important result given by the IKS spectrum is the double structure of this emission, which shows two distinct maxima, at 9.0 and 11.2 μm. Another striking point is the strength of the whole emission, which reaches about twice the continuum level at 9 and 11 μm. These two facts fully confirm the results given by Bregman *et al.* (1987) from data recorded in December 1985, with the KAO and with ground-based telescopes. There is also some evidence for a double structure in the 8–12 μm ground-based data recorded by Bouchet *et al.* (1987) on January 26, 1986, but the feature was weaker at that time (about 1.5 times the continuum level). As pointed out by Hanner *et al.* (1987), the silicate feature showed a general increase as the heliocentric distance decreased, but also showed important time variations, both in intensity and in spectral shape.

Bregman *et al.* (1987) have shown that the comet 8–12 μm feature can be closely matched by the combination of spectra of interplanetary dust particles containing olivines, pyroxenes, and a small amount of layer lattice silicates. Olivine has to be present to fit the 11.2-μm peak. This result implies that, unlike the silicates observed in the interstellar medium which show no structure in their emission band and are believed to be amorphous, the cometary silicates of P/Halley (or a fraction of them) are crystalline. These silicates might have been formed at a higher temperature than interstellar dust particles were, which could lead to constraints on the history of grains accreted by cometary nuclei. However, this conclusion is probably premature, since it relies on the simple comparison of two spectra in a restricted wavelength region. As shown by attempts at quantitative fits to comet Halley emissions (Crifo 1988b,c), the problem of producing a dust chemical composition compatible with both the *in situ* measured mass spectra and with the complete (near ultraviolet to far infrared) emission spectrum is yet unresolved.

4.2.4. Absolute Flux Observed with IKS

The flux observed at 10 μm with our instrument at a distance of 40,000 km to the nucleus, in a field of view of 1°, is 10^{-5} W cm^{-2} μm^{-1} sr^{-1}, or 2.5×10^{-9} W cm^{-2} μm^{-1}. This can be compared with ground-based observations recorded on March 6.85 at IRTF by Hanner *et al.* (1987) with a field of view of 6.8 arcsec. Assuming an isotropic expansion of dust at constant velocities, the IKS value can be converted for the

conditions of the IRTF observation (geocentric distance of 1.14 AU). Assuming the flux to be proportional to the linear diameter of the field of view and inversely proportional to the square of the distance D to the comet, we can derive a value of 1.1×10^{-15} W cm^{-2} μm^{-1} for the IKS flux converted to the IRTF conditions, whereas the IRTF measurement leads to a flux of about 1.5×10^{-15} W cm^{-2} μm^{-1} at 10 μm. The small discrepancy between the IKS and IRTF fluxes may be due to temporal variations (the IKS data were recorded 12 hr before the IRTF observation) or to calibration uncertainties.

5. CONCLUSIONS

The IKS spectroscopic experiment has observed the infrared spectrum of the near-nucleus region of comet Halley from 2.5 to 12 μm. The signatures of several molecular species have been detected in the spectral region 2.5–5 μm:

1. The strong signature of the 2.7-μm band of water. The corresponding production rate is 10^{30} sec^{-1}. In addition, H_2O ice is probably present in absorption at 2.9 μm.
2. The 4.3-μm band of carbon dioxide, detected for the first time in a comet, with a production rate of 2.7×10^{28} sec^{-1}.
3. A strong and broad emission at 3.2–3.5 μm, also detected for the first time in a comet, attributed to the C–H stretch in hydrocarbons, in both the saturated and the unsaturated form. It is not yet clear whether these hydrocarbons are gaseous or in solid phase (as polycyclic aromatic hydrocarbons or the organic mantles of small grains) or both. If gaseous, these hydrocarbons would require a carbon abundance in the comet comparable to that of water, which seems unrealistic. If in the solid phase, their carbon abundance would be smaller than the total abundance of carbon observed in radicals such as CH, CN, C_2, and C_3.
4. Weaker emission at 4.3 μm, attributed to formaldehyde (production rate $\sim 4 \times 10^{28}$ sec^{-1}).
5. The $v(1 - 0)$ band of carbon monoxide, possibly present at 4.6 and 4.7 μm. The CO production rate observed in the infrared is definitely smaller than that observed in the UV, suggesting that the main source of CO is not the nucleus, but dissociation of other molecules (including H_2CO) or grains.
6. Marginal features, which might be due to OCS (4.8 μm) and some CN-bearing molecules (4.5 μm).

The 6- to 12-μm part of the spectrum is dominated by the silicate emission between 8 and 12 μm and shows no emission feature between 6 and 8 μm. The silicate emission has a characteristic double structure with peaks at 9 and 11.2 μm, which implies the presence of olivine. This result means that, in comet Halley, silicates (or at least a fraction of them) are in a crystalline form, in contrast with interstellar silicates generally observed in the amorphous form.

All the molecular spectral signatures show, at least in first order, a D^{-1} variation law with distance, as expected for parent products. Therefore, all the detected species come from the nucleus or the inner coma region, and not from the progressive dissociation of heavier species, or from sputtering at the surface of the grains. The results of the IKS experiment do not give a complete view of the composition of the volatile fraction of comet Halley, because the instrument could not observe species that do not have permitted infrared bands (such as N_2 or rare gases) or that do not have strong bands in its spectral range (such as NH_3). However, a comparison with the observations of radicals in the visible and UV ranges and with the *in situ* mass spectrometer measurements shows that the IKS experiment has not missed many volatile materials: among lacking parent species, N_2 and NH_3 have abundance upper limits of 10 and 4%, respectively (Eberhardt *et al.* 1987, Krankowsky *et al.* 1986); sulfurous molecules should be less than 2% (Azoulay and Festou 1986).

We now have an almost complete

scheme of the chemical composition of cometary volatiles which seems to confirm the model of cometary nuclei proposed by Whipple (1950) many years ago: a conglomerate of dust and ices, water ice being largely dominant. An interesting question is whether the secondary species are contained in clathrate hydrates, as was suggested by Delsemme and Swings (1952). If they are, cometary ice would be relatively stable, and its sublimation would be governed by water–ice sublimation. Clathrate hydrates can accommodate a maximum of 18% in number of guest molecules in their cavities. The abundance of CO-bearing molecules (CO, CO_2, H_2CO) observed by IKS is already ~10%. With hydrocarbons, N_2, possibly NH_3, rare gases, and other minor species, the limit may well be reached. It must also be noted that hydrocarbons heavier than pentane cannot be contained in clathrate hydrates. Therefore, it seems likely that a fraction of cometary volatiles are not in clathrate hydrates, but in the form of ices of their own, or of molecules adsorbed in amorphous ice (Bar-Nun *et al.* 1987, Schmitt and Klinger 1987). The most volatile of these species could sublimate first, and be responsible for cometary activity at large heliocentric distances.

The comparison of elemental abundances in cometary volatiles and in interstellar matter (Encrenaz *et al.* 1987, 1988) supports the idea that cometary nuclei form through condensation of material in interstellar clouds. It is remarkable that both cometary material and interstellar matter contain carbonaceous material responsible for nearly similar emission features at 3.2–3.5 μm. We now have a wealth of clues allowing us to test models of comet nucleus formation.

The actual chemical composition of cometary nuclei may be complex, with possibly all intermediates between simple polyatomic molecules (H_2O, CO, CO_2, . . .) and large molecules such as PAH or polymers. The IKS experiment, as well as other *in situ* observations, has only revealed the very few most abundant parent molecules and an indication of the presence of unidentified hydrocarbons. Definite identifications of parent molecules at the abundance level of 1% or less are still lacking, if one excepts the radio detection of HCN. The greatest progress in this topic will be achieved in a few decades with comet sample return missions. In the meantime, decisive advances could be realized by remote sensing through infrared spectroscopy, either from cometary probes or Earth-based and Earth-orbital observatories.

ACKNOWLEDGMENTS

We thank the members of the French and Soviet technical teams for their highly efficient cooperative effort during the development, testing, and operation of the IKS instrument. We are grateful to Dr. E. Gérard and Dr. D. Malaise for their scientific support during the early phases of the project. Financial support was provided by the Centre National d'Etudes Spatiales.

REFERENCES

ALLEN, D. A., AND D. T. WICKRAMASINGHE 1987. Discovery of organic grains in comet Wilson. *Nature* **329,** 615–616.

ANDRESEN, P. A., G. S. ONDREY, B. TITZE, AND E. W. ROTHE 1984. Nuclear and electron dynamics in the photodissociation of water. *J. Chem. Phys.* **80,** 2548–2569.

ARDUINI, M., J. P. BIBRING, S. CAZES, M. COMBES, N. CORON, J. F. CRIFO, T. ENCRENAZ, R. GISPERT, D. HARDUIN, J. M. LAMARRE, AND D. MALAISE 1982. The comet Halley flyby IR sounder "IKS." *Adv. Space Res.* **2**(4), 113–122.

AZOULAY, G., AND M. C. FESTOU 1986. The abundance of sulphur in comets. In *Asteroids, Comets, Meteors II* (C.-I. Lagerqvist *et al.*, Eds.), pp. 273–277. Uppsala Univ. Press, Uppsala.

BAAS, F., T. R. GEBALLE, AND D. M. WALTHER 1986. Spectroscopy of the 3.4 micron emission feature in comet Halley. *Astrophys. J.* **311,** L97–L101.

BAR-NUN, A., J. DROR, E. KOCHAVI, AND D. LAUFER 1987. Amorphous water ice and its ability to trap gases. *Phys. Rev. B* **35,** 2427–2435.

BELLAMY, L. J. 1975. *The Infrared Spectra of Complex Molecules,* Vol. 1. Chapman Hall, London.

BIBRING, J.-P., S. CAZES, J. CHARRA, M. COMBES, N. CORON, B. COUGRAND, J.-F. CRIFO, J. CROVISIER, C. EMERICH, T. ENCRENAZ, R. GISPERT, B. GONDET, G. GUYOT, D. HARDUIN, J.-M. LAMARRE, G. LEVANTI, C. MAUREL, D. PARISOT, F. ROCART, P. SALVETAT, AND A. SOUFFLOT 1984. The instrument

IKS and its calibration. *Adv. Space Res.* **4**(9), 273–276.

BISIKALO, D. V., C. V. REPIN, AND V. C. STRELNITSKIJ 1987. A method to determine the temperature of the neutral coma. *In Problems of Applied Mathematics in Aeronomy,* Keldysh Institute of Applied Mathematics, USSR Academy of Sciences, Moscow. [in Russian]

BOCKELÉE-MORVAN, D. 1987. A model for the excitation of water in comets. *Astron. Astrophys.* **181,** 169–181.

BOCKELÉE-MORVAN, D., AND J. CROVISIER 1985. Possible parents for the cometary CN radical: Photochemistry and excitation conditions. *Astron. Astrophys.* **151,** 90–100.

BOCKELÉE MORVAN, D., AND J. CROVISIER 1986. Modelling the excitation conditions of the water molecule in comets. In *Asteroids, Comets, Meteors II* (C.-I. Lagerqvist *et al.,* Eds.), pp. 279–282. Uppsala Univ. Press, Uppsala.

BOCKELÉE-MORVAN, D., AND J. CROVISIER 1987a. The 2.7 μm water band of comet P/Halley: Interpretation of observations by an excitation model. *Astron. Astrophys.* **187,** 425–430.

BOCKELÉE-MORVAN, D., AND J. CROVISIER 1987b. The role of water in the thermal balance of the coma. In *Symposium on the Diversity and Similarity of Comets,* ESA SP-278, pp. 235–240.

BOCKELÉE-MORVAN, D., J. CROVISIER, A. BAUDRY, D. DESPOIS, M. PERAULT, W. M. IRVINE, F. P. SCHLOERB, AND D. SWADE 1984. Hydrogen cyanide in comets: Excitation conditions and radio observations of comet IRAS-Araki-Alcock 1983d. *Astron. Astrophys.* **141,** 411–418.

BOCKELÉE-MORVAN, D., J. CROVISIER, D. DESPOIS, T. FORVEILLE, E. GÉRARD, J. SCHRAML, AND C. THUM 1987. Molecular observations of comets P/Giacobini-Zinner 1984e and P/Halley 1982i at millimetre wavelengths. *Astron. Astrophys.* **180,** 253–262.

BOUCHET, P., A. CHALABAEV, A. DANKS, T. ENCRENAZ, N. EPCHTEIN, AND T. LE BERTRE 1987. Infrared photometry of comet P/Halley before perihelion. *Astron. Astrophys.* **174,** 288–294.

BREGMAN, J. D., H. CAMPINS, F. C. WITTEBORN, D. M. WOODEN, D. M. RANK, L. J. ALLAMANDOLA, M. COHEN, AND A. G. G. M. TIELENS 1987. Airborne and groundbased spectrophotometry of comet P/Halley from 5 to 13 micrometers. *Astron. Astrophys.* **187,** 616–620.

BROOKE, T. Y., AND R. F. KNACKE 1987. *Proceedings of the Workshop on Infrared Observations of Comets Halley and Wilson,* Ithaca, August 10–12, 1987.

BROOKE, T., R. KNACKE, T. OWEN, AND A. TOKUNAGA 1987. Comet Wilson (1986l). IAU Circ. No 4399.

CAMPINS, H., J. D. BREGMAN, F. C. WITTEBORN, D. H. WOODEN, D. M. RANK, L. J. ALLAMANDOLA, M. COHEN, AND A. G. TIELENS 1986. Airborne spectrophotometry of comet Halley from 5 to 9 microns. In *20th ESLAB Symposium on the exploration of Halley's comet,* ESA SP-250, Vol. II, pp. 121–124.

CHIBA, C., AND C. SAGAN 1987. Infrared emission by organic grains in the coma of comet Halley. *Nature* **330,** 350–353.

CHIN, G., AND H. A. WEAVER 1984. Vibrational and rotational excitation of CO in comets: Non-equilibrium calculations. *Astrophys. J.* **285,** 858–869.

COKER, D. F., R. E. MILLER, AND R. O. WATTS 1985. The infrared predissociation spectra of water clusters. *J. Chem. Phys.* **82,** 3554–3562.

COMBES, M., V. I. MOROZ, J. F. CRIFO, J. M. LAMARRE, J. CHARRA, N. F. SANKO, A. SOUFFLOT, J. P. BIBRING, S. CAZES, N. CORON, J. CROVISIER, C. EMERICH, T. ENCRENAZ, R. GISPERT, A. V. GRIGORIEV, G. GUYOT, V. A. KRASNOPOLSKY, YU. V. NIKOLSKY, AND F. ROCARD 1986a. Infrared sounding of comet Halley from Vega 1. *Nature* **321,** 266–268.

COMBES, M., V. I. MOROZ, J. F. CRIFO, J. M. LAMARRE, J. CHARRA, N. F. SANKO, A. SOUFFLOT, J. P. BIBRING, S. CAZES, N. CORON, J. CROVISIER, C. EMERICH, T. ENCRENAZ, R. GISPERT, A. V. GRIGORIEV, G. GUYOT, V. A. KRASNOPOLSKY, YU. V. NIKOLSKY, AND F. ROCARD 1986b. Infrared sounding of comet Halley from the VEGA probe: Preliminary results of the IKS experiment. [in Russian] *Pisma Astron. Zh.* **12,** 611–615 (English translation: *Sov. Astron. Lett.* **12,** 257–259).

COMBES, M., V. MOROZ, J. F. CRIFO, J. P. BIBRING, N. CORON, J. CROVISIER, T. ENCRENAZ, N. SANKO, A. GRIGORIEV, D. BOCKELÉE-MORVAN, R. GISPERT, C. EMERICH, J. M. LAMARRE, F. ROCARD, V. KRASNOPOLSKY, AND T. OWEN 1986c. The 2.5 to 5 microns spectrum of comet Halley from the IKS instrument of Vega. *Adv. Space Res.* **5**(12), 127–131.

COMBES, M., V. MOROZ, J. F. CRIFO, J. P. BIBRING, N. CORON, J. CROVISIER, T. ENCRENAZ, N. SANKO, A. GRIGORIEV, D. BOCKELÉE-MORVAN, R. GISPERT, C. EMERICH, J. M. LAMARRE, F. ROCARD, V. KRASNOPOLSKY, AND T. OWEN 1986d. Detection of parent molecules in comet Halley from the IKS-Vega experiment. In *20th ESLAB Symposium on the Exploration of Halley's Comet,* ESA SP-250, Vol. 1, pp. 353–358.

CRIFO, J. F. 1981. Infrared sounding of comet Halley from the flyby Venera Halley probes. In *The Solar System and Its Exploration,* ESA SP-164, pp. 229–244.

CRIFO, J. F. 1987. Improved gas-kinetic treatment of cometary water sublimation and recondensation: Application to comet P/Halley. *Astron. Astrophys.* **187,** 438–450.

CRIFO, J. F. 1988a. Water polymers in the coma of comet Halley. Submitted for publication.

CRIFO, J. F. 1988b. Are cometary dust mass loss rates

deduced from optical emissions reliable? In *Proceedings of the Xth European Regional Astronomy meeting of the IAU, Tchecoslovac*. Academy of Science Press, Prague.

CRIFO, J. F. 1988c. Cometary dust sizing: Comparison between optical and in-situ sampling techniques. *Partic. Char.* **5,** in press.

CRIFO, J. F., AND C. EMERICH 1985. Model for an icy halo in comets. In *Ices in the Solar System* (J. Klinger *et al.*, Eds.), pp. 429–442. Reidel, Dordrecht.

CROVISIER, J. 1984. The water molecule in comets: Fluorescence mechanisms and thermodynamics of the inner coma. *Astron. Astrophys.* **130,** 361–372.

CROVISIER, J. 1987. Rotational and vibrational synthetic spectra of linear parent molecules in comets. *Astron. Astrophys. Suppl.* **68,** 223–258.

CROVISIER, J., AND T. ENCRENAZ 1983. Infrared fluorescence of molecules in comets: The general synthetic spectrum. *Astron. Astrophys.* **126,** 170–182.

CROVISIER, J., AND J. LE BOURLOT 1983. Infrared and microwave fluorescence of carbon monoxide in comets. *Astron. Astrophys.* **123,** 61–66.

CURTIS, C. C., C. Y. FAN, K. C. HSIEH, D. M. HUNTEN, W.-H. IP, E. KEPPLER, A. K. RICHTER, G. UMLAUFT, V. V. AFONIN, A. V. DYACHKOV, J. ERO, JR., AND A. J. SOMOGYI 1986. Comet Halley neutral gas density profile along the VEGA 1 trajectory measured by NGE. In *20th ESLAB Symposium on the Exploration of Halley's Comet*, ESA SP-250, Vol. I, pp. 391–395.

DANKS, A. C., T. ENCRENAZ, P. BOUCHET, T. LE BERTRE, AND A. CHALABAEV 1987. The spectrum of comet P/Halley from 3.0 to 4.0 μm. *Astron. Astrophys.* **184,** 329–332.

DELSEMME A. H., AND P. SWINGS 1952. Hydrates de gaz dans les noyaux cométaires et les grains interstellaires. *Ann. Astrophys.* **15,** 1–6.

D'HENDECOURT, L. B., AND L. J. ALLAMANDOLA 1986. Time dependent chemistry in dense molecular clouds. III. Infrared band cross sections of molecules in the solid state at 10 K. *Astron. Astrophys. Suppl.* **64,** 453–467.

D'HENDECOURT, L. B., L. J. ALLAMANDOLA, R. J. A. GRIM, AND J. M. GREENBERG 1986. Time-dependent chemistry in dense molecular clouds. II. Ultraviolet photoprocessing and infrared spectroscopy of grain mantles. *Astron. Astrophys.* **158,** 119–134.

EBERHARDT, P., D. KRANKOWSKY, W. SCHULTE, U. DOLDER, P. LAMMERZAHL, J. J. BERTHELIER, J. WOWERIES, U. STUBBEMANN, R. R. HODGES, J. H. HOFFMAN, AND J. M. ILLIANO 1987. The CO and N_2 abundance in comet P/Halley. *Astron. Astrophys.* **187,** 481–484.

EMERICH, C., J. M. LAMARRE, V. I. MOROZ, M. COMBES, N. F. SANKO, YU. V. NIKOLSKY, F. ROCARD, R. GISPERT, N. CORON, J. P. BIBRING, T. ENCRENAZ, AND J. CROVISIER 1987. Temperature and size of the nucleus of comet P/Halley deduced from IKS infrared Vega 1 measurements. *Astron. Astrophys.* **187,** 839–842.

ENCRENAZ, T., J. CROVISIER, M. COMBES, AND J. F. CRIFO 1982. A theoretical study of comet Halley's spectrum in the infrared range. *Icarus* **51,** 660–664.

ENCRENAZ, T., L. D'HENDECOURT, AND J. L. PUGET 1988. On the interpretation of the 3.2–3.5 micron emission feature in the spectrum of comet Halley: Abundances in P/Halley and in interstellar matter. *Astron. Astrophys.*, in press.

ENCRENAZ, T., J. L. PUGET, J. P. BIBRING, M. COMBES, J. CROVISIER, C. EMERICH, L. D'HENDECOURT, AND F. ROCARD 1987. On the interpretation of the 3 μm emission feature in the spectrum of comet Halley: Abundances in comet Halley and in interstellar matter. In *Symposium on the Diversity and Similarity of Comets*, ESA SP-278, pp. 369–376.

FELDMAN, P. D., M. F. A'HEARN, M. C. FESTOU, L. A. MCFADDEN, H. A. WEAVER, AND T. N. WOODS 1986. Is CO_2 responsible for the outbursts of comet Halley? *Nature* **324,** 433–436.

FESTOU, M. C., P. D. FELDMAN, M. F. A'HEARN, C. ARPIGNY, C. B. COSMOVICI, A. C. DANKS, L. A. MCFADDEN, R. GILMOZZI, P. PATRIARCHI, G. P. TOZZI, M. K. WALLIS, AND H. A. WEAVER 1986. IUE observations of comet Halley during the Vega and Giotto encounters. *Nature* **321,** 361–363.

FINKEL, A. G. 1966. Experimental and theoretical study of absolute intensities in the infrared spectra of gaseous hydrocarbons. VI. *Opt. Spectrosc.* **20,** 432–435.

GRIGORIEV, A. V. 1987. Analysis of the 3.35 μm hydrocarbon band in the spectrum of Comet Halley observed by the IKS experiment of VEGA mission. *Kosmich. Issled.* **25,** 810–814. [in Russian]

GRINGAUZ, K. I., T. I. GOMBOSI, A. P. REMIZOV, I. APATHY, I. SZEMEREY, M. I. VERIGIN, L. I. DENCHIKOVA, A. V. DYACHVOV, E. KEPPLER, I. N. KLIMENKO, A. K. RICHTER, A. J. SOMOGYI, K. SZEGO, S. SZENDRO, M. TATRALLYAY, A. VARGA, AND G. A. VLADIMIROVA 1986. First in situ plasma and neutral gas measurements at comet Halley. *Nature* **321,** 282–285.

HANNER, M. S. 1984. Comet Cernis: Icy grains at last? *Astrophys. J.* **277,** L75–L78.

HANNER, M. S., D. K. AITKEN, R. KNACKE, S. MCCORKLE, P. F. ROCHE, AND A. T. TOKUNAGA 1985. Infrared spectrophotometry of comet IRAS-Araki-Alcock (1983d): A bare nucleus revealed? *Icarus* **62,** 97–109.

HANNER, M. S., A. T. TOKUNAGA, W. F. GOLISH, D. M. GRIEP, AND C. D. KAMINSKY 1987. Infrared emission from P/Halley's dust coma during March 1986. *Astron. Astrophys.* **187,** 653–660.

HUEBNER, W. F. 1985. The photochemistry of comets. In *The Photochemistry of Atmospheres* (J. S.

Levine, Ed.), pp. 437–495. Academic Press, New York.

HUEBNER, W. F. 1987. First polymer in space identified in comet Halley. *Science* **327,** 628–629.

HUEBNER, W. F., D. C. BOICE, AND C. M. SHARP 1987. Polyoxymethylene in comet Halley. *Astrophys. J.* **320,** L49–L52.

HUSSON, N., A. CHEDIN, N. A. SCOTT, D. BAILLY, G. GRANNER, N. LACOME, A. LEVY, C. ROSSETTI, G. TARRAGO, C. CAMY-PEYRET, J. M. FLAUD, A. BAUER, J. M. COLMONT, N. MONNANTEUIL, J. C. HILICO, G. PIERRE, L. LOETE, J. P. CHAMPION, L. S. ROTHMAN, L. R. BROWN, G. ORTHON, P. VARANASI, C. P. RINSLAND, M. A. H. SMITH, AND A. GOLDMAN 1986. The GEISA spectroscopic line parameters data bank in 1984. *Ann. Geophys. A* **4**(2), 185–190.

KISSEL, J., D. E. BROWNLEE, K. BUCHLER, B. C. CLARK, H. FECHTIG, E. GRUN, K. HORNUNG, E. B. IGENBERGS, E. K. JESSBERGER, F. R. KRUEGER, H. KUCZERA, J. A. M. MCDONNEL, G. M. MORFILL, J. RAHE, G. H. SCHWEHM, Z. SEKANINA, N. G. UTTERBACK, H. J. VOLK, AND H. A. ZOOK 1986a. Composition of comet Halley dust particles from Giotto observations. *Nature* **321,** 336–337.

KISSEL, J., R. Z. SAGDEEV, J. L. BERTAUX, V. N. ANGAROV, J. AUDOUZE, J. E. BLAMONT, K. BUCHLER, E. N. EVLANOV, H. FECHTIG, M. N. FOMENKOVA, H. VON HOERNER, N. A. INOGAMOV, V. N. KHROMOV, W. KNABE, F. R. KRUEGER, Y. LANGEVIN, V. B. LEONAS, A. C. LEVASSEUR-REGOURD, G. G. MANAGADZE, S. N. PODKOLZIN, V. D. SHAPRIO, S. R. TABALDYEV, AND B. V. ZUBKOV 1986b. Composition of comet Halley dust particles from Vega observations. *Nature* **321,** 280–282.

KITAMURA, Y., AND T. YAMAMOTO 1986. Hydrodynamic study of condensation and sublimation of ice particles in cometary atmospheres. *Icarus* **68,** 266–275.

KNACKE, R. F., T. Y. BROOKE, AND R. R. JOYCE 1986. Observations of 3.2–3.6 micron emission features in comet Halley. *Astrophys. J.* **310,** L49–L54.

KRANKOWSKY, D., P. LÄMMERZAHL, I. HERRWERTH, J. WOWERIES, P. EBERHARDT, U. DOLDER, U. HERRMANN, W. SCHULTE, J. J. BERTHELIER, J. M. ILLIANO, R. R. HODGES, AND J. H. HOFFMAN 1986. *In situ* gas and ion measurements at comet Halley. *Nature* **321,** 326–329.

KRASNOPOLSKY, V. A., V. I. MOROZ, A. A. KRYSKO, V. S. JEGULEV, A. YU. TKACHUK, M. GOGOSHEV, TS. GOGOSHEVA, G. MOREELS, J. CLAIREMIDI, AND J. P. PARISOT 1986. Near infrared spectroscopy of comet Halley by the VEGA-2 three channel spectrometer. In *20th ESLAB on the Exploration of Halley's Comet,* ESA SP-250, Vol. I, pp. 459–463.

KRASNOPOLSKY, V. A., AND A. YU. TKACHUK 1987. Curves of growth of emission lines in cometary spectra: Implications to H_2O and OH bands of comet P/Halley. *Astron. Astrophys.* **187,** 431–434.

KRISHNA SWAMY, K. S., S. A. SANDFORD, L. J. ALLAMANDOLA, F. C. WITTEBORN, AND J. D. BREGMAN 1988. A multicomponent model of the infrared emission from comet Halley. *Icarus* **75,** 351–370.

LABS, D., AND H. NECKEL 1968. The radiation of the solar photosphere from 2000 Å to 100 μ. *Z. Astrophys.* **69,** 1–73.

LÄMMERZAHL, P., D. KRANKOWSKY, R. R. HODGES, U. STUBBERMAN, J. WOWERIES, I. HERRWERTH, J. J. BERTHELIER, J. M. ILLIANO, P. EBERHARDT, U. DOLDER, W. SCHULTE, AND J. H. HOFFMAN 1986. Expansion velocity and temperatures of gas and ions measured in the coma of comet Halley. In *20th ESLAB Symposium on the Exploration of Halley's Comet,* ESA SP-250, Vol. I, pp. 179–182.

LÉGER, A., AND L. D'HENDECOURT 1987. Identification of PAHs in astronomical IR spectra—implications. In *Polycyclic Aromatic Hydrocarbons and Astrophysics* (A. Léger *et al.* Eds.), pp. 223–254. Reidel, Dordrecht.

LÉGER, A., AND J. L. PUGET 1984. Identification of the "unidentified" IR emission features of interstellar dust? *Astron. Astrophys.* **137,** L5–L8.

MITCHELL, D. L., R. P. LIN, K. A. ANDERSON, C. W. CARLSON, D. W. CURTIS, A. KORTH, H. RÉME, J. A. SAUVAUD, C. D'HUSTON, AND D. A. MENDIS 1987. Evidence for chain molecules enriched in carbon, hydrogen, and oxygen in comet Halley. *Science* **237,** 626–628.

MOREELS, G., M. GOGOSHEV, V. A. KRASNOPOLSKY, J. CLAIREMIDI, M. VINCENT, J. P. PARISOT, J. L. BERTAUX, J. E. BLAMONT, M. C. FESTOU, TS. GOGOSHEVA, S. SARGOISHEV, K. PALASOV, V. I. MOROZ, A. A. KRYSKO, AND V. VANYSEK 1986. Near-ultraviolet and visible spectrophotometry of comet Halley from Vega 2. *Nature* **321,** 271–273.

MOROZ, V. I., M. COMBES, J. P. BIBRING, N. CORON, J. CROVISIER, T. ENCRENAZ, J. F. CRIFO, N. SANKO, A. V. GRIGORIEV, D. BOCKELÉE-MORVAN, R. GISPERT, Y. V. NIKOLSKY, C. EMERICH, J. M. LAMARRE, F. ROCARD, V. A. KRASNOPOLSKY, AND T. OWEN 1987a. Detection of parent molecules in comet Halley from the IKS-Vega experiment. *Astron. Astrophys.* **187,** 513–518.

MOROZ, V. I., M. COMBES, A. V. GRIGORIEV, J. F. CRIFO, T. ENCRENAZ, J. CROVISIER, J. P. BIBRING, N. SANKO, N. CORON, D. BOCKELÉE-MORVAN, YU. V. NIKOLSKY, R. GISPERT, J. M. LAMARRE, V. A. KRASNOPOLSKY, C. EMERICH, F. ROCARD, AND T. OWEN 1987b. Results of the IKS experiment: 1. Infrared emission of parent molecules in comet Halley. *Kosmich. Issled.* **25,** 781–792. [in Russian]

MUMMA, M. J., H. A. WEAVER, H. P. LARSON, D. S. DAVIS, AND M. WILLIAMS 1986. Detection of water vapor in Halley's comet. *Science* **232,** 1523–1528.

NIKOLSKY, YU. V., C. EMERICH, J. M. LAMARRE, N. F. SANKO, M. COMBES, V. I. MOROZ, J. CROVISIER, T. ENCRENAZ, F. ROCARD, A. V. GRIGORIEV, R. GISPERT, J. P. BIBRING, A. V. KISELEV, AND N. CORON 1987. Results of the IKS experiment: 2. Infrared radiometry of Comet Halley nucleus. *Kosmich. Issled.* **25,** 793–809. [in Russian]

OISHI, M., K. KAWARA, Y. KOBAYASHI, T. MAIHARA, K. NOGUCHI, H. OKUDA, S. SATO, T. IIJIMA, AND T. ONO 1978. Infrared observations of comet West 1975. I. Observational results. *Publ. Astron. Soc. Japan* **30,** 149–159.

SCHLOERB, F. P., W. M. KINZEL, D. A. SWADE, AND W. M. IRVINE 1987. Observations of HCN in comet P/Halley. *Astron. Astrophys.* **187,** 475–480.

SCHMITT, B., AND J. KLINGER 1987. Different trapping mechanisms of gases by water ice and their relevance for comet nuclei. In *Symposium on the Diversity and Similarity of Comets,* ESA SP-278, pp. 613–619.

SELLGREN, K. 1984. The near-infrared continuum emission of visual reflection nebulae. *Astrophys. J.* **277,** 623–633.

SINGH, P. D., AND A. DALGARNO 1987. Photodissociation lifetimes of CH and CD radicals in comets. In *Symposium on the Diversity and Similarity of Comets,* ESA SP-278, pp. 177–180.

SNYDER, L. E., P. PALMER, AND I. DE PATER 1988. Radio detection of formaldehyde emission from comet Halley. *Astron. J.*, in press.

STEWART, A. I. F. 1987. Pioneer Venus measurements of H, O, and C production in comet P/Halley near perihelion. *Astron. Astrophys.* **187,** 369–374.

SVERDLOV, L. M., M. A. KOVNER, AND E. P. KRAINOV 1970. *Vibrational Spectra of Polyatomic Molecules.* Nauka, Moscow. [in Russian]

TOKUNAGA, A. T., T. NAGATA, AND R. G. SMITH 1987. Detection of a new emission band at 2.8 μm in comet P/Halley. *Astron. Astrophys.* **187,** 519–522.

WEAVER, H. A., AND M. J. MUMMA 1984. Infrared molecular emission from comets. *Astrophys. J.* **276,** 782–797.

WHIPPLE, F. 1950. A comet model. I. The acceleration of comet Encke. *Astrophys. J.* **111,** 375–394.

WICKRAMASINGHE, D. T., AND D. A. ALLEN 1986. Discovery of organic grains in comet Halley. *Nature* **323,** 44–46.

WOODS, T. N., P. D. FELDMAN, K. F. DYMOND, AND D. J. SAHNOW 1986. Rocket ultraviolet spectroscopy of comet Halley and abundance of carbon monoxide and carbon. *Nature* **324,** 436–438.

WYCKOFF, S., S. TEGLER, P. A. WEHINGER, H. SPINRAD, AND M. J. S. BELTON 1988. Abundances in comet Halley at the time of the spacecraft encounters. *Astrophys. J.*, in press.

YAMAMOTO, T. 1982. Evaluation of infrared line emission from constituent molecules of cometary nuclei. *Astron. Astrophys.* **109,** 326–330.